Impact of dust addition on the metabolism of Mediterranean plankton communities and carbon export under present and future conditions of pH and temperature

Frédéric Gazeau[1], France Van Wambeke[2], Emilio Marañón[3], María Pérez-Lorenzo[3], Samir Alliouane[1], Christian Stolpe[1], Thierry Blasco[1], Nathalie Leblond[4], Birthe Zäncker[5,6], Anja Engel[6], Barbara Marie[7], Julie Dinasquet[7,8], Cécile Guieu[1]

[1] Sorbonne Université, CNRS, Laboratoire d'Océanographie de Villefranche, LOV, 06230 Villefranche-sur-Mer, France
[2] Aix-Marseille Université, Université de Toulon, CNRS/INSU, IRD, Mediterranean Institute of Oceanography (MIO), UM 110, 13288, Marseille, France
[3] Department of Ecology and Animal Biology, Universidade de Vigo, 36310 Vigo, Spain
[4] Sorbonne Université, CNRS, Institut de la Mer de Villefranche, IMEV, 06230 Villefranche-sur-Mer, France
[5] The Marine Biological Association of the UK, PL1 2PB Plymouth, United Kingdom
[6] GEOMAR Helmholtz Centre for Ocean Research, Kiel, Germany
[7] CNRS, Sorbonne Université, Laboratoire d'Océanographie Microbienne, LOMIC, F-66650 Banyuls-sur-Mer, France
[8] Scripps Institution of Oceanography, University of California San Diego, USA

Correspondence to: Frédéric Gazeau (frederic.gazeau@imev-mer.fr)

Keywords: Mediterranean Sea; Atmospheric deposition; Plankton community metabolism; Carbon export; Ocean acidification; Ocean warming

Abstract

Although atmospheric dust fluxes from arid as well as human-impacted areas represent a significant source of nutrients to surface waters of the Mediterranean Sea, studies focusing on the evolution of the metabolic balance of the plankton community following a dust deposition event are scarce and none were conducted in the context of projected future levels of temperature and pH. Moreover, most of the experiments took place in coastal areas. In the framework of the PEACETIME project, three dust-addition perturbation experiments were conducted in 300-L tanks filled with surface seawater collected in the Tyrrhenian Sea (TYR), Ionian Sea (ION) and in the Algerian basin (FAST) onboard the R/V "*Pourquoi Pas?*" in late spring 2017. For each experiment, six tanks were used to follow the evolution of chemical and biological stocks, biological activity and particle export. The impacts of a dust deposition event simulated at their surface were followed under present environmental conditions and under a realistic climate change scenario for 2100 (ca. + 3 °C and -0.3 pH units). The tested waters were all typical of stratified oligotrophic conditions encountered in the open Mediterranean Sea at this period of the year, with low rates of primary production and a metabolic balance towards net heterotrophy. The release of nutrients after dust seeding had very contrasting impacts on the metabolism of the communities, depending on the station investigated. At TYR, the release of new nutrients was followed by a negative impact on both particulate and dissolved ^{14}C-based production rates, while heterotrophic bacterial production strongly increased, driving the community to an even more heterotrophic state. At ION and FAST, the efficiency of organic matter export due to mineral/organic aggregation processes was lower than at TYR and likely related to a lower quantity/age of dissolved organic matter present at the time of the seeding and a smaller

45 production of DOM following dust addition. This was also reflected by lower initial
46 concentrations in transparent exopolymer particles (TEP) and a lower increase in TEP
47 concentrations following the dust addition, as compared to TYR. At ION and FAST, both the
48 autotrophic and heterotrophic community benefited from dust addition, with a stronger relative
49 increase in autotrophic processes observed at FAST. Our study showed that the potential positive
50 impact of dust deposition on primary production depends on the initial composition and
51 metabolic state of the investigated community. This impact is constrained by the quantity of
52 nutrients added in order to sustain both the fast response of heterotrophic prokaryotes and the
53 delayed one of primary producers. Finally, under future environmental conditions, heterotrophic
54 metabolism was overall more impacted than primary production, with the consequence that all
55 integrated net community production rates decreased with no detectable impact on carbon
56 export, therefore reducing the capacity of surface waters to sequester anthropogenic CO_2.

1. Introduction

Low Nutrient Low Chlorophyll (LNLC) areas represent 60% of the global ocean surface area (Longhurst et al., 1995; McClain et al., 2004). Although phytoplankton production in these areas is limited by the availability of nitrogen, phosphorus and iron, it accounts for 50% of global carbon export (Emerson et al., 1997; Roshan and DeVries, 2017). Atmospheric dust fluxes represent a significant source of these nutrients to surface waters in LNLC regions and as such could play a significant role in stimulating primary production (e.g. Bishop et al., 2002; Guieu et al., 2014b; Jickells and Moore, 2015), potentially increasing the efficiency of the biological pump in the sequestration of atmospheric CO_2. However, as heterotrophic prokaryotes have been shown to outcompete phytoplankton during nutrient addition experiments (e.g. Guieu et al., 2014a; Mills et al., 2008; Thingstad et al., 2005), dust deposition could induce even stronger enhancements of heterotrophic bacterial production and/or respiration rates thereby reducing net atmospheric CO_2 drawdown and the potential for carbon export outside the euphotic zone (Guieu et al., 2014b). Indeed, several experiments conducted in the Atlantic Ocean and in the Mediterranean Sea have shown a fast and dominant effect of dust additions on heterotrophic bacterioplankton metabolism (Herut et al., 2005, 2016; Lekunberri et al., 2010; Marañón et al., 2010; Pulido-Villena et al., 2008, 2014). However, to the best of our knowledge, no study focused on the evolution of the metabolic balance of the plankton community after such a dust event in the open sea. The metabolic balance (or net community production, NCP) is defined as the difference between gross primary production (GPP) of autotrophic organisms and community

78 respiration (CR) of both autotrophic and heterotrophic organisms, revealing the capacity of
79 surface waters to absorb atmospheric CO_2.

80 The Mediterranean Sea is a perfect example of LNLC regions and receives anthropogenic
81 aerosols originating from industrial and domestic activities from all around the basin and other
82 parts of Europe and pulses of natural inputs from the Sahara (Desboeufs, 2021). These
83 atmospheric depositions, mostly in the form of pulsed inputs (Loÿe-Pilot and Martin, 1996),
84 provide new nutrients (Guieu et al., 2010; Kouvarakis et al., 2001; Markaki et al., 2003; Ridame
85 and Guieu, 2002) to the surface waters with fluxes that are of the same order of magnitude as
86 riverine inputs (Powley et al., 2017). These significant nutrient enrichments likely support
87 primary production especially during the stratification period (Bonnet et al., 2005; Ridame and
88 Guieu, 2002). However, no clear correlation between dust and ocean color have been evidenced
89 from long series of satellite observations (Guieu and Ridame, 2020). This raises the question on
90 which compartment (autotrophic or heterotrophic) benefits the most from these transient relieves
91 in nutrient (N, P) limitation.

92 In response to ocean warming and increased stratification, LNLC areas are expected to
93 expand in the future (Irwin and Oliver, 2009; Polovina et al., 2008) due to lower nutrient supply
94 from sub-surface waters (Behrenfeld et al., 2006). Furthermore, dust deposition could increase in
95 the future due to desertification (Moulin and Chiapello, 2006), although so far the trend for
96 deposition remains uncertain because the drying of the Mediterranean basin might also induce
97 less wet deposition over the basin (Laurent et al., 2021). Nevertheless, whether the fluxes
98 increase or not in the coming decades and centuries, new nutrients from atmospheric sources will
99 play an important role in a surface mixed layer even more stratified and isolated from the deeper
100 nutrient-rich layer. The question remains on how plankton metabolism and carbon export would

101 respond in a warmer and more acidified ocean. Indeed, with an average annual anthropogenic
102 CO_2 uptake, during the period 2010 to 2019, of 2.5 ± 0.6 GtC (~22.9% of anthropogenic
103 emissions; Friedlingstein et al., 2020), the oceans substantially contribute towards slowing down
104 the increase in atmospheric CO_2 concentrations, and therefore towards limiting terrestrial and
105 ocean warming. However, this massive CO_2 input induces global changes in seawater chemistry
106 referred to as "ocean acidification" because increased CO_2 concentration lowers seawater pH
107 (i.e. increases its acidity).

108 Although the response of plankton metabolism to ocean warming has been shown to be
109 highly dependent on resource availability (Lewandowska et al., 2014), both for heterotrophic
110 bacteria (Lopez-Urrutia and Moran, 2007) and phytoplankton (Marañón et al., 2018), it has been
111 suggested that ocean warming will substantially weaken the ocean biological CO_2 sink in the
112 future as a consequence of stronger increase in remineralization than in photosynthesis
113 processes, following the metabolic theory of ecology (MTE; Brown et al., 2004; Gillooly et al.,
114 2001). Ocean acidification alone has been shown to exert no or very limited influence on
115 plankton metabolism in the Mediterranean Sea (Maugendre et al., 2017a; Mercado et al., 2014).
116 To the best of our knowledge, only Maugendre et al. (2015) studied the combined impact of
117 ocean warming and acidification on plankton metabolism in the Mediterranean Sea. They found
118 a very limited impact of ocean acidification on the plankton community and a positive impact of
119 warming on small phytoplankton species (e.g. Cyanobacteria) with a potential decrease of the
120 export and energy transfer to higher trophic levels. Their study was conducted under nutrient
121 depleted conditions (Maugendre et al., 2017b). Hence, there is still a need to assess the combined
122 impact of warming and acidification on the metabolic balance of plankton communities in this
123 region, following a transient relief in nutrient availability.

So far there has been no attempt to evaluate the evolution of plankton metabolism and carbon export following atmospheric deposition in the context of future levels of temperature and pH. Such experiments were conducted in the frame of the PEACETIME project (ProcEss studies at the Air-sEa Interface after dust deposition in the MEditerranean sea; http://peacetime-project.org/) during the cruise on board the R/V "*Pourquoi Pas?*" in May/June 2017 (Guieu et al., 2020a, b). The project aimed at extensively studying and parameterizing the chain of processes occurring in the Mediterranean Sea after atmospheric deposition, especially of Saharan dust, and to put them in perspective of on-going environmental changes. During this cruise, three perturbation experiments were conducted in 300-L tanks filled with surface seawater collected in the Tyrrhenian Sea (TYR), Ionian Sea (ION) and in the Algerian basin (FAST; Fig. 1). Six tanks were used to follow the evolution of chemical and biological stocks, biological activity and export, following a wet dust deposition event simulated at their surface, both under present environmental conditions and following a realistic climate change scenario for 2100 (ca. + 3 °C and -0.3 pH units; IPCC, 2013). A companion paper presents the general setup of the experiments and the impacts of dust under present and future environmental conditions on nutrients and biological stocks (Gazeau et al., 2021). In this paper, we show that the effects of dust deposition on biological stocks were highly different between the three investigated stations and could not be attributed to differences in their degree of oligotrophy but rather to the initial metabolic state of the community. We further demonstrated that ocean acidification and warming did not drastically modify the composition of the autotrophic assemblage with all groups positively impacted by warming and acidification. Here, we focus on the impacts of dust seeding on plankton metabolism (e.g. primary production, heterotrophic prokaryote production) and carbon export.

2. Material and Methods

2.1. General set-up

The general set-up of the experiments is fully detailed in Gazeau et al. (2021). Briefly, three experiments were performed at the long duration stations TYR, ION and FAST during the Peacetime cruise onboard R/V "*Le Pourquoi Pas?*" (Fig. 1). During these experiments (3 to 4 days each), seawater was incubated in 300-L tanks (Fig. S1) installed in a temperature-controlled container, in which the irradiance spectrum and intensity can be finely controlled and in which future ocean acidification and warming conditions can be fully reproduced. The tanks were made of high-density polyethylene (HDPE) and were trace-metal free in order to avoid contaminations, with a height of 1.09 m, a diameter of 0.68 m, a surface area of 0.36 m^2 and a volume of 0.28 m^3. The conical base of the tanks was equipped with a sediment trap that was left open during the duration of the experiments and removed at the end. The experimental protocol comprised two unmodified control tanks (C1 and C2), two tanks enriched with Saharan dust (D1 and D2) and two tanks enriched with Saharan dust and maintained simultaneously under warmer (+ 3 ºC) and acidified (-0.3 pH unit) conditions (G1 and G2). At the three stations, tanks were always filled at the end of the day before the start of the experiments: TYR (17/05/2017), ION (25/05/2017) and FAST (02/06/2017). The tanks were filled by means of a large peristaltic pump (Verder© VF40 with EPDM hose, flow of 1200 L h^{-1}) collecting seawater below the base of the boat (depth of ~ 5 m), used to supply continuously surface seawater to a series of instruments during the entire campaign. While filling the tanks, seawater was sampled for the measurements of selected parameters (sampling time = t-12h). After filling the tanks, seawater was slowly warmed

overnight using 500 W heaters, controlled by temperature-regulation units (COREMA©), in G1 and G2 to reach an offset of + 3 °C. ^{13}C-bicarbonate was added to all tanks at 4:00 am (all times in local time) and G1 and G2 were acidified by addition of CO_2-saturated filtered (0.2 µm) seawater (~1.5 L in 300 L; collected when filling the tanks at each station) at 4:30 am to reach a pH offset of -0.3. Sampling for many parameters took place prior to dust seeding (sampling time = t0). Dust seeding was performed between 7:00 and 9:00 in tanks D1, D2, G1 and G2. The same dust analog was used and the same dust flux was simulated as for the DUNE 2009 experiments described in Desboeufs et al. (2014). Briefly, the fine fraction (< 20 µm) of Saharan soils collected in southern Tunisia, which is a major source of dust deposition over the northwestern Mediterranean basin, was used in the seeding experiments. The particle size distribution showed that 99% of particles had a size smaller than 0.1 µm, and that particles were mostly made of quartz (40%), calcite (30%) and clay (25%; Desboeufs et al., 2014). This collected dust underwent an artificial chemical aging process by addition of nitric and sulfuric acid (HNO_3 and H_2SO_4, respectively) to mimic cloud processes during atmospheric transport of aerosol with anthropogenic acid gases (Guieu et al., 2010, and references therein). To mimic a wet flux event of 10 g m^{-2}, 3.6 g of this analog dust were quickly diluted into 2 L of ultrahigh-purity water (UHP water; 18.2 MΩ cm^{-1} resistivity), and sprayed at the surface of the tanks using an all-plastic garden sprayer (duration = 30 min). The intensity of this simulated wet deposition event (i.e. 10 g m^{-2}) represents a high but realistic scenario, as several studies reported even higher short wet deposition events in this area of the Mediterranean Sea (Bonnet and Guieu, 2006; Loÿe-Pilot and Martin, 1996; Ternon et al., 2010).

Depending on the considered parameter or process, seawater sampling was conducted 1 h (t1h), 6 h (t6h), 12 h (t12h), 24 h (t24h), 48 h (t48h) and 72 h (t72h) after dust additions in all

three experiments with an additional sample after 96 h (t96h) at FAST). Acid-washed silicone tubes were used for transferring the water collected from the tanks to the different vials or containers.

2.2. Stocks

2.2.1. Dissolved and particulate organic carbon

The concentration of dissolved organic carbon (DOC) was determined from duplicate 10 mL GF/F (pre-combusted, Whatman©) filtered subsamples that were transferred to pre-combusted glass ampoules, acidified with H_3PO_4 (final pH = 2) and sealed. The sealed glass ampoules were stored in the dark at room temperature until analysis at the Laboratoire d'Océanographie Microbienne (LOMIC). DOC measurements were performed on a Shimadzu© TOC-V-CSH (Benner and Strom, 1993). Prior to injection, DOC samples were sparged with CO_2-free air for 6 min to remove inorganic carbon. Sample (100 µL) were injected in triplicate and the analytical precision was 2%. Standards were prepared with acetanilid.

Seawater samples for measurements of particulate organic carbon concentrations (POC; 2 L) were taken at t-12h, t0, t12h, t24h, t48h and t72h (or t96h for station FAST), filtered on pre-combusted GF/F membranes, dried at 60 °C and analyzed at the Laboratoire d'Océanographie de Villefranche (LOV, France) following decarbonatation with a drop of HCl 2N, on an elemental analyzer coupled with an isotope ratio mass spectrometer (EA-IRMS; Vario Pyrocube-Isoprime 100, Elementar©). A caffeine standard (IAEA-600) was used to calibrate the EA-IRMS.

2.2.2. Total hydrolysable carbohydrates and amino acids

For total hydrolysable carbohydrates and amino acids, samples were taken at t0, t6h, t24h, t48h and t72h at all stations. For total hydrolysable carbohydrates (TCHO) > 1 kDa, samples (20 mL) were filled into pre-combusted glass vials (8 h, 500 °C) and stored at -20 °C pending analysis. Prior to analysis, samples were desalted with membrane dialysis (1 kDa MWCO, Spectra Por) at 1 °C for 5 h. Samples were subsequently hydrolyzed for 20 h at 100 °C with 0.8 M HCl final concentration followed by neutralization using acid evaporation (N_2, for 5 h at 50 °C). TCHO were analysed at GEOMAR using high performance anion exchange chromatography with pulsed amperometric detection (HPAEC-PAD), on a Dionex© ICS 3000 ion chromatography system following the procedure of Engel and Händel (2011). Two replicates per TCHO sample were analyzed. The variation coefficient between duplicate measurements was 7% on average.

For total hydrolysable amino acids (TAA), samples (5 mL) were filled into pre-combusted glass vials (8 h, 500 °C) and stored at -20 °C. Samples were hydrolyzed at 100 °C for 20 h with 1 mL 30% HCl (Suprapur®, Merck) added to 1 mL of sample, and neutralized by acid evaporation under vacuum at 60 °C in a microwave. Samples were analyzed by high performance liquid chromatography (HPLC) using an Agilent 1260 HPLC system following a modified version of established methods (Dittmar et al., 2009; Lindroth and Mopper, 1979). Separation of 13 amino acids with a C18 column (Phenomenex Kinetex, 2.6 µm, 150 x 4.6 mm) was obtained after in-line derivatization with o-phthaldialdehyde and mercaptoethanol. A gradient with solvent A containing 5 % acetonitrile (LiChrosolv, Merck, HPLC gradient grade) in sodium dihydrogenphosphate (Suprapur®, Merck) buffer (pH 7.0) and solvent B being acetonitrile was used for analysis. A gradient from 100% solvent A to 78% solvent A was produced in 50 min. Two replicates per TAA sample were analyzed. The variation coefficient

234 between duplicate measurements was 8% on average. For TCHO and TAA, instrument blanks
235 were performed with MilliQ water. The detection limit was calculated as 3x the blank value,
236 which is ~1 nmol L^{-1} for both parameters.

237 2.2.3. Transparent exopolymer particles

238 Samples for transparent exopolymer particles (TEP) were taken at t0, t24h and t72h at all
239 stations. The abundance and area of TEP were microscopically measured following the
240 procedure given in Engel (2009). Samples of 10-50 mL were directly filtered under low vacuum
241 (< 200 mbar) onto a 0.4 µm Nucleopore membrane (Whatman©) filter, stained with 1 mL Alcian
242 Blue solution (0.2 g l^{-1} w/v) for 3 s and rinsed with MilliQ water. Filters were mounted on
243 Cytoclear© slides and stored at -20 °C until analysis. Two filters per sample with 30 images each
244 were analyzed using a Zeiss Axio Scope.A1 (Zeiss©) and an AxioCam MRc (Zeiss©). The
245 pictures with a resolution of 1388 x 1040 pixels were saved using AxioVision LE64 Rel. 4.8
246 (Zeiss©). All particles larger than 0.2 μm^2 were analyzed. ImageJ© and R were subsequently
247 used for image analysis (Schneider et al., 2012). The coefficients of variation between duplicate
248 filters averaged 28%.

249 Filters prepared with 10 mL MilliQ water instead of samples served as a blank. Blanks
250 were always <1% of sample values. The carbon content of TEP (TEP-C) was estimated after
251 Mari (1999) using the size-dependent relationship:

252 $$TEP\text{-}C = a \, \Sigma_i \, n_i \, r_i^D \quad (1)$$

253 with n_i being the number of TEP in the size class i and r_i being the mean equivalent spherical
254 radius of the size class. The constant $a = 0.25 * 10^{-6}$ (µg C) and the fractal dimension of

aggregates $D = 2.55$ were used as proposed by Mari (1999). To relate to organic carbon concentration in seawater, data for TEP-C are given as μmol L^{-1}.

2.3. Processes

2.3.1. Dissolved and particulate ^{14}C incorporation rates

The photosynthetic production of particulate (< 0.2-2 μm and > 2 μm size fractions) and dissolved organic matter was determined from samples taken at t0, t24h, t48h and t72h (or t96h at station FAST) with the ^{14}C-uptake technique. From each tank, four polystyrene bottles (70 mL; three light and one dark bottles) were filled with sampled seawater and amended with 40 μCi of $NaH^{14}CO_3$. Bottles were incubated for 8 h in two extra 300 L tanks maintained under similar light and temperature regimes as in the experimental tanks (ambient temperature for C1, C2, D1 and D2 and ambient temperature + 3 °C for G1 and G2). Incubations were terminated by sequential filtration of the sample through polycarbonate filters (pore sizes 2 μm and 0.2 μm, 47 mm diameter) using low-pressure vacuum. Filters were exposed for 12 h to concentrated HCl fumes to remove non-fixed, inorganic ^{14}C, and then transferred to 4 mL plastic scintillation vials to which 3.5 mL of scintillation cocktail (Ultima Gold XR, Perkin Elmer©) were added. For the measurement of dissolved primary production, a 5 mL aliquot of each sampling bottle was filtered, at the end of incubation, through a 0.2 μm polycarbonate filter (25 mm diameter). This filtration was conducted, under low-pressure vacuum, in a circular filtration manifold that allows the recovery of the filtrate into 20 mL scintillation vials. The filtrates were acidified with 200 μL of 50% HCl and maintained in an orbital shaker for 12 h. Finally, 15 mL of liquid scintillation cocktail was added to each sample. All filter and filtrate samples were measured onboard in a

liquid scintillation counter (Packard© 1600 TR). ^{14}C-based production rates (PP; in µg C L^{-1} h^{-1}) were calculated as:

$$PP = C_T \times \left(\frac{DPM_{sample} - DPM_{dark}}{DPM_{added} \times t}\right) \quad (2)$$

where C_T is the concentration of total dissolved inorganic carbon (µg C L^{-1}), DPM_{sample} and DPM_{dark} are the radioactivity counts in the light and dark bottle, respectively, DPM_{added} is the radioactivity added to each sample, and t is the incubation time (h).

The percentage extracellular release (PER%) was calculated as:

$$PER\% = \frac{PPd}{PPd + PPp} \times 100 \quad (3)$$

where PPd refers to ^{14}C-based dissolved production and PPp refers to ^{14}C-based particulate production (sum of < 2 and > 2 µm size fractions).

2.3.2. Integrated ^{13}C incorporation

Addition of ^{13}C-bicarbonate ($NaH^{13}CO_3$ 99%; Sigma-Aldrich©) was performed in each tank before t0 in order to increase the isotopic level (δ^{13}C signature) of the dissolved inorganic carbon pool to ca. 350‰. We followed the time evolution of the δ^{13}C signature in dissolved inorganic carbon (δ^{13}C-C_T), dissolved organic carbon (δ^{13}C-DOC) and particulate organic carbon pools (δ^{13}C-POC). For the analysis of the actual δ^{13}C-C_T, 60 mL of sampled seawater (at t-12h, t0, t12h, t24h, t48h and t72h; + t96h at station FAST) was gently transferred to glass vials avoiding bubbles. Vials were sealed after being poisoned with 12 µL saturated $HgCl_2$ and stored upside-down at room temperature in the dark pending analysis. At the University of Leuven, a helium headspace (5 mL) was created in the vials and samples were acidified with 2 mL of

296 phosphoric acid (H_3PO_4, 99%). Samples were left to equilibrate overnight to transfer all C_T to
297 gaseous CO_2. Samples were injected in the carrier gas stream of an EA-IRMS (Thermo©
298 EA1110 and Delta V Advantage), and data were calibrated with NBS-19 and LSVEC standards
299 (Gillikin and Bouillon, 2007).

300 At the same frequency as for $\delta^{13}C$-C_T, samples for $\delta^{13}C$-DOC were filtered online (see
301 above), transferred to 40 mL pre-cleaned borosilicate amber EPA vials with septa caps (PTFE-
302 lined silicone) and stored in the dark pending analysis at the Ján Veizer Stable Isotope
303 Laboratory (Ottawa, Canada).

304 At t-12h, t0, t12h, t24h, t48h and t72h (or t96h at station FAST), the $\delta^{13}C$-POC was
305 obtained based on the same measurements as described above for POC, on an elemental analyzer
306 coupled with an isotope ratio mass spectrometer (EA-IRMS; Vario Pyrocube-Isoprime 100,
307 Elementar©).

308 Carbon isotope data are expressed in the delta notation (δ) relative to Vienna Pee Dee
309 Belemnite (VPDB) standard (Schimmelmann et al., 2016). The carbon isotope ratio was
310 calculated as:

311 $$R_{sample} = \left(\frac{\delta^{13}C_{sample}}{1000} + 1\right) \text{x } R_{VPDB} \quad (4)$$

312 with $R_{VPDB} = 0.011237$.

2.3.2. Community metabolism (oxygen light-dark method)

At the same frequency as for ^{14}C incorporation, from each tank, a volume of 2 L was sampled in plastic bottles and distributed in 15 biological oxygen demand (BOD; 60 mL) borosilicate bottles. Five BOD bottles were immediately fixed with Winkler reagents (initial O_2 concentrations), five BOD bottles were incubated in the dark for the measurement of community respiration (CR) in two incubators maintained respectively at ambient temperature for C1, C2, D1 and D2 and at ambient temperature + 3 °C for G1 and G2. Additionally, five BOD bottles were incubated for the measurement of net community production (NCP) in the same tanks as described above for ^{14}C-incorporation. Upon completion of the incubations (24 h), samples were fixed with Winkler reagents. Within one day, O_2 concentrations were measured using an automated Winkler titration technique with potentiometric endpoint detection. Analyses were performed on board with a Metrohm© Titrando 888 and a redox electrode (Metrohm© Au electrode). Reagents and standardizations were similar to those described by Knap et al. (1996). NCP and CR were estimated by regressing O_2 values against time, and CR was expressed as negative values. Since CR is estimated from the oxygen evolution (consumption) in bottles (negative sign), GPP corresponds to, and was calculated as GPP = NCP - CR.

Gross primary production (GPP) was calculated as the difference between NCP and CR. The combined standard errors were calculated as:

$$SE_{xy} = \sqrt{SE_x^2 + SE_y^2} \quad (5)$$

2.3.4. Heterotrophic prokaryotic production and ectoenzymatic activities

At all sampling times, heterotrophic bacterial production (BP, *sensus stricto* referring to heterotrophic prokaryotic production) was determined onboard using the microcentrifuge method with the ^{3}H- leucine (^{3}H-Leu) incorporation technique to measure protein production (Smith and Azam, 1992). The detailed protocol is in Van Wambeke et al. (2021). Briefly, triplicate 1.5 mL samples and one blank were incubated in the dark for 1-2 h in two thermostated incubators maintained respectively at ambient temperature for C1, C2, D1 and D2 and at ambient temperature +3 °C for G1 and G2. Incubations were ended by the addition of TCA to a final concentration of 5%, followed by three runs of centrifugation at 16000 g for 10 min. Pellets were rinsed with TCA 5% and ethanol 80%. A factor of 1.5 kg C mol leucine^{-1} was used to convert the incorporation of leucine to carbon equivalents, assuming no isotopic dilution (Kirchman et al., 1993).

Ectoenzymatic activities were measured fluorometrically, using fluorogenic model substrates that were L-leucine-7-amido-4-methyl-coumarin (Leu-MCA) and 4 methylumbelliferyl – phosphate (MUF-P) to track aminopeptidase activity (LAP) and alkaline phosphatase activity (AP), respectively (Hoppe, 1983). Stocks solutions (5mM) were prepared in methycellosolve and stored at -20 °C. Release of the products of LAP and AP activities, MCA and MUF, were followed by measuring increase of fluorescence (exc/em 380/440 nm for MCA and 365/450 nm for MUF, wavelength width 5 nm) in a VARIOSCAN LUXmicroplate reader calibrated with standards of MCA and MUF solutions. For measurements, 2 mL of unfiltered samples from the tanks were supplemented with 100

µL of a fluorogenic substrate solution diluted so that different concentrations were dispatched in a black 24-well polystyrene plate in duplicate (0.025, 0.05, 0.1, 0.25, 0.5, 1 µM for MUF-P, 0.5, 1, 5, 10, 25 µM for MCA-leu). Incubations were carried out in the same thermostatically controlled incubators than those used for BP and reproducing temperature levels in the experimental tanks. Incubations lasted up to 12 h long with a reading of fluorescence every 1 to 2 h, depending on the intended activities. The rate was calculated from the linear part of the fluorescence versus time relationship. Boiled-water blanks were run to check for abiotic activity. From varying velocities obtained, we determined the parameters Vm (maximum hydrolysis velocity) and Km (Michaelis-Menten constant which reflects enzyme affinity for the substrate) by fitting the data using a non-linear regression on the following equation:

$$V = V_m \, x \frac{S}{K_m + S} \quad (6)$$

where V is the hydrolysis rate and S the fluorogenic substrate concentration added.

2.3.5. Inorganic and organic material export

At the end of each experiment (t72h for TYR and ION and t96 h for FAST, after artificial dust seeding), the sediment traps were removed, closed and stored with formaldehyde 4%. Back in the laboratory, after the swimmers were removed, the samples were rinsed by centrifugation in MilliQ water (3 times) to remove sea salt and then freeze-dried. The total amount of material collected was first weighted to measure the total exported flux. Several aliquots were then weighted to measure the following components: total carbon and organic carbon, lithogenic and biogenic silicates and calcium. Total carbon was measured on an elemental analyzer coupled

with an isotope ratio mass spectrometer (EA-IRMS; Vario Pyrocube-Isoprime 100, Elementar©). Particulate organic carbon (POC) was measured in the same way after removing inorganic carbon by acidification with HCl 2N. Particulate inorganic carbon (PIC) was obtained by subtracting particulate organic carbon from particulate total carbon. Calcium concentrations were measured by ICP-OES (Inductively Coupled Plasma - Optic Emission Spectrometry; Perkin-Elmer© Optima 8000) on acid digested samples (the organic matrix was removed by HNO_3 while the mineral aluminosilicate matrix was eliminated with HF). Biogenic silica (BSi) and Lithogenic silica (LSi) were measured by colorimetry (Analytikjena© Specor 250 plus spectrophotometer) after a NaOH/HF digestion, respectively (Mosseri et al., 2005). The carbonate fraction of the exported material was determined from particulate calcium concentrations (%$CaCO_3$ = 5/2 x (%Ca). The organic matter fraction was calculated as 2 x %POC (Klaas and Archer, 2002) The lithogenic fraction was calculated as [total mass – (organic matter + $CaCO_3$ + opal) and was very comparable to the lithogenic fraction calculated from LSi (taking Si concentration in dust analog used for seeding from Desboeufs et al., 2014; ca. 11.9%). In the controls, the amount of material exported was low and the entire content of the traps was filtered in order to measure total mass and organic matter mass fluxes. Measured concentrations on blank filters were 1.1 % of the average concentration of the sample (thus negligible). For all analyses, replicates agreement was on average 0.3 - 2.3 %. No standard deviation were estimated as we analyse only two aliquots over the three when the two first measurements agree (<5% difference) and that was the case for all the samples analysed in this study.

2.4. Data processing

All metabolic rates were integrated over the duration of the experiments using trapezoidal integrations and the relative changes (in %) in tanks D and G as compared to the controls (average between C1 and C2) were computed following:

$$\text{Relative change} = \left(\frac{\text{Rate}_{\text{Treatment}} - \text{Rate}_{\text{Controls}}}{\text{Rate}_{\text{Controls}}}\right) \times 100 \quad (7)$$

Where $\text{Rate}_{\text{Treatment}}$ is the integrated rate measured in treatments D and G (D1, D2, G1 or G2) and $\text{Rate}_{\text{Controls}}$ is the averaged integrated rates between the duplicate controls (treatment C). Daily rates of ^{14}C-based production were computed from hourly rates assuming a 14 h daylight period. As incubations performed from samples taken at t0 (before dust addition) do not represent what happened in the tanks between t0 and t24h, as a first assumption, we considered a linear evolution between these rates and those measured from samples at t24h, and recomputed an average value for the time interval t0 - t24 h. At FAST, no incubations were performed for ^{14}C incorporation and oxygen metabolism between t72h and t96h, again an average rate between rates measured from samples taken at t48h and t96h was used for this time interval. Since bacterial respiration rates were not measured, bacterial growth efficiency (BGE, expressed as a percentage) was estimated based on BP (carbon units) and community respiration (CR, oxygen units). As BP was determined more often than CR during the first 48 h, hourly BP rates were integrated using trapezoidal integrations during the time period when CR was measured. We assumed that heterotrophic prokaryotes were responsible for 70% of CR (BR/CR ratio; Lemée et al., 2002) and used a respiratory quotient (RQ) of 0.8 (del Giorgio and Williams, 2005), following the equation:

$$\text{BGE} = \left(\frac{\text{BP}}{\text{CR} \times \frac{\text{BR}}{\text{CR}}\text{ratio} \times \text{RQ} + \text{BP}}\right) \times 100 \quad (8)$$

When BP varied following an exponential growth, we calculated growth rates (μ_{BP}) from linear least square regression of ln BP rates versus time.

3. Results

3.1. Initial conditions

Initial conditions in terms of the chemical and biological standing stocks measured while filling the tanks at the three stations are fully described in Gazeau et al. (2021). Briefly, the three experiments were conducted with surface seawater collected during stratified oligotrophic conditions typical of the open Mediterranean Sea at this period of the year (Table 1). Nevertheless, a dust event took place nine days before sampling at station TYR as evidenced from particulate inventory of lithogenic proxies (Al, Fe) in the water column (Bressac et al., 2021), likely stimulating phytoplankton growth before the start of the experiment. Nitrate + nitrite (NO_x) concentrations were maximal at station FAST with a NO_x to dissolved inorganic phosphate (DIP) molar ratio of ~ 4.6. Very low NO_x concentrations were observed at stations TYR and ION (14 and 18 nmol L^{-1}, respectively). DIP concentrations were the highest at station TYR (17 nmol L^{-1}) and the lowest at the most eastern station (ION, 7 nmol L^{-1}). Consequently, the lowest NO_x:DIP ratio was measured at TYR (0.8), compared to ION and FAST (2.8 and 4.6, respectively). Silicate ($Si(OH_4)$) concentrations were similar at TYR and ION (~1 µmol L^{-1}) and the lowest at FAST (~0.6 µmol L^{-1}). Both POC and DOC concentrations were the highest at station TYR (12.9 and 72.2 µmol L^{-1}, respectively) and the lowest at FAST (6.0 and 69.6 µmol L^{-1}, respectively). Very low and similar concentrations of chlorophyll *a* were measured at the three stations (0.063 - 0.072 µg L^{-1}). Phytoplankton communities at stations TYR and ION were dominated by Prymnesiophytes followed by Cyanobacteria, while, at station FAST, the phytoplanktonic community was clearly dominated by photosynthetic prokaryotes. At all three stations, the proportion of pigments representative of larger species was very small (< 5%;

Gazeau et al., 2021). Heterotrophic prokaryotes were the most abundant at station FAST (6.15 x 10^5 cells mL^{-1}) and the least abundant at station ION (2.14 x 10^5 cells mL^{-1}).

Relatively similar ^{14}C-based particulate production rates were measured at the start of the experiments (t0) in the control tanks (C1 and C2) at station ION and FAST (ca. 0.014 - 0.015 µg C L^{-1} h^{-1}). At both stations, ca. 80% of the production was attributed to larger (> 2 µm) cells and the percentage of extracellular release (%PER) did not exceed 45%. Lower rates were estimated at station TYR (total particulate production of 0.08 µg C L^{-1} h^{-1}) from which 87.5% was due to large cells > 2 µm. A larger amount of ^{14}C incorporation was released as dissolved organic matter at station TYR compared to the two other stations (PER ca. 60%). Metabolic balance derived from oxygen measurements showed that, at all three stations, the community was net heterotrophic with a higher degree of heterotrophy at station TYR (NCP were -1.9, -0.2, -0.8 µmol O_2 L^{-1} d^{-1} at TYR, ION and FAST, respectively, as measured in the controls from seawater sampled at t0). CR and GPP rates were respectively the highest and the lowest at station TYR compared to the other two stations. Finally, BP rates were the highest at station FAST (35.8 ng C L^{-1} h^{-1}), intermediate at ION (26.1 ng C L^{-1} h^{-1}) and the lowest at TYR (21.3 ng C L^{-1} h^{-1}).

3.2. Changes in biological stocks

DOC concentrations showed a general positive trend during the three experiments and a large variability between duplicates (Fig. 2). This variability appeared as soon as 1 h after dust seeding (t1h) while the range of variation at t0 (before dust seeding) was rather moderate (difference between minimal and maximal values in all tanks of 1.3, 6.2 and 4.3 µmol C L^{-1} at station TYR, ION and FAST, respectively). As a consequence of this variability, no clear impact of dust seeding (D) could be highlighted at station TYR and FAST. Indeed, DOC concentrations in the two duplicates (D1 and D2) were higher than values in the controls (C1 and C2) in only

33% of the samples along the experiments (after dust seeding). In contrast, at station ION, DOC concentrations appeared impacted by dust seeding as higher concentrations were almost systematically (83% of the time after dust seeding) measured for this treatment as compared to control tanks at the same time. At all stations, this impact was somewhat exacerbated under conditions of temperature and pH projected for 2100 (G1 and G2) as DOC concentrations were almost all the time higher in these tanks than in control tanks (83 - 100% of the samples after dust seeding, depending on the station).

Total hydrolysable carbohydrates and amino acids concentrations along the three experiments are shown in Fig. S2. TCHO concentrations were quite variable between tanks before dust seeding (t0; 649 - 954, 569 - 660 and 600 - 744 nmol L^{-1} at station TYR, ION and FAST, respectively) and no visible impact of the treatments were visible at station TYR (TCHO tended to decrease everywhere). In contrast, at station ION and FAST, values in dust amended tanks increased and appeared higher than in control tanks towards the end of the experiments although the large variability between duplicates tended to mask this potential effect. An impact of dust seeding was much clearer for TAA concentrations that showed larger increases throughout the three experiments in tanks D1 and D2 as compared to control tanks, this effect being exacerbated for warmer and acidified tanks (G1 and G2). The ratio between TAA and DOC concentrations (Fig. 2) showed positive trends in tanks D and G during all three experiments with a clear distinction between treatments at the end of the experiments (G > D > C). The strongest increase was observed at station FAST in tanks G where final TAA/DOC ratios were above 3%.

Particulate organic carbon (POC) concentrations strongly decreased at all stations between t-12h and t0, this decrease being the largest at station TYR where concentrations

488 dropped from 25.7 to 9.6 - 13.2 µmol C L^{-1} (Fig. 3). After dust seeding, POC concentrations did
489 not show clear temporal trends for the three experiments although a slight general increase could
490 be observed at station FAST. Furthermore, no impact of dust seeding and warming/acidification
491 could be observed on POC dynamics. While concentrations of transparent exopolymer particles
492 (TEP-C) were rather constant through time in control tanks at the three stations, a large increase
493 was observed in dust-amended tanks (D and G) with TEP-C reaching values up to ~2 µmol C L^{-1}
494 in tank G1 at station TYR after 24 h (i.e. ~17% of POC concentration, Fig. 3). In all cases except
495 for tank G2 at station ION, TEP-C further decreased towards the end of the experiments although
496 concentrations remained well above those observed in the controls. As the variability between
497 duplicated tanks G was rather high, no impact of warming/acidification on TEP dynamics could
498 be highlighted at the three stations.

499 3.3. Changes in metabolic rates

500 ^{14}C-based particulate production rates as measured during the different time intervals at
501 the three stations were low in control tanks (maximal total particulate production of 0.34 µg L^{-1}
502 h^{-1} at station FAST) and did not show any particular temporal dynamics (Fig. 4). In these tanks,
503 the vast majority of particulate production was attributed to cells above 2 µm (65 - 89%). The
504 percentage of extracellular release (%PER) was overall maximal at station TYR and minimal at
505 station FAST with a tendency to decrease with time at the three stations although large variations
506 were observed between duplicates.

507 Dust addition alone did not have any clear positive impact on all ^{14}C-based rates at
508 station TYR, with even an observable decrease in production rates from larger cells (> 2 µm)
509 compared to the controls. In contrast, at this station, dust seeding under warmer and acidified
510 conditions (tanks G) had a positive effect on particulate production rates, this effect being

511 particularly visible for cells < 2 µm and to a lesser extent on dissolved production with a general
512 decrease of %PER. An important discrepancy between the duplicates of treatment G was
513 observable at the end of the experiment with much larger rates measured in tank G2.
514 In contrast to station TYR, an enhancement effect of dust addition was clearly visible at
515 station ION where all rates increased towards the end of this experiment reaching a maximal
516 total particulate production of 0.6 - 0.7 µg L^{-1} h^{-1} in tanks D1 and D2. Since this positive effect
517 was similar between small and larger cells, dust addition alone had no effect on the partitioning
518 of production at this station, with cells > 2 µm representing ~80% of total production. Although
519 being also positively impacted and increasing with time, dissolved production appeared less
520 sensitive than particulate production leading to an overall decrease of %PER at station ION
521 following dust addition. These positive impacts of dust seeding on ^{14}C-based particulate
522 production rates were even more visible at this station under warmer and acidified conditions
523 (tanks G) with maximal rates more than doubled compared to those measured under present
524 conditions of temperature and pH (1.5 - 1.6 µg L^{-1} h^{-1}). Dust seeding under warmer and acidified
525 conditions had a slight impact on the partitioning of particulate production at station ION with
526 smaller cells benefiting the most from these conditions. %PER remained between 20 and 30%.
527 At station FAST, similarly to station ION, total particulate production rates were clearly
528 enhanced by dust addition (tanks D) reaching maximal values during the incubation time interval
529 t48 - 56h. No clear increase was observed for total particulate production on the next incubation
530 (t96 - 120h) while production rates of cells larger than 2 µm increased and rates of smaller cells
531 decreased. However, in contrast to station ION, there was much less impact of
532 warming/acidification on all measured rates at station FAST although rates measured on smaller
533 cells (< 2 µm) did not decrease at the end of the experiment as observed under present

534 environmental conditions. %PER under both present conditions of temperature and pH (tanks D)
535 decreased during this experiment reaching values lower than in the controls and in tanks G.
536 The initial enrichment of the tanks in ^{13}C-bicarbonate led to an increase in the ^{13}C
537 signature of dissolved inorganic carbon (δ^{13}C-C_T) of above 300‰, with generally lower values
538 measured in warmer and acidified tanks (G; Fig. S3). After this initial enrichment, δ^{13}C-C_T levels
539 decreased linearly in all tanks. At stations TYR and ION, the isotopic signature of dissolved
540 organic carbon (δ^{13}C-DOC; Fig. S3) increased with time, although these increases were rather
541 low and limited to ~ 4‰ over the course of the experiments. In contrast to station TYR, at ION,
542 an enhanced incorporation of ^{13}C into DOC was visible after 24 h in tanks D and G in
543 comparison to control tanks. A similar observation was done at station FAST, especially at the
544 end of the experiment, although much more variability was observed at this station.
545 The incorporation of ^{13}C into particulate organic carbon (δ^{13}C-POC) is shown in Fig. 5.
546 At all stations, δ^{13}C-POC increased with time but reached lower enrichment levels at station
547 TYR as compared to ION and FAST. At station TYR, incorporation rates appeared smaller in
548 dust-amended tanks under present environmental conditions (tanks D). As for ^{14}C-based
549 production rates, an important discrepancy was observed between duplicates under future
550 conditions of temperature and pH (tanks G) with much higher final δ^{13}C-POC at the end of the
551 experiment in tank G2. At station ION, enrichment levels obtained at the end of the experiment
552 were more important in dust-amended tanks reaching maximal levels of 73‰ in tank G2 at t72h.
553 This enhancement effect was even more visible at station FAST with maximal enrichment levels
554 of 146‰ (tank D2 at t96h). Since no sampling occurred at t72h, these enrichment levels cannot
555 be directly compared to what was measured at station TYR and ION. However, by interpolating

556 values at t72h assuming a linear increase between these time intervals, enrichment levels
557 appeared similar although slightly higher for tanks D between station ION and FAST.
558 NCP rates as measured using the O_2 light-dark method showed that, under control
559 conditions, the communities remained the vast majority of the time throughout the three
560 experiments in a net heterotrophic state (NCP < 0; Fig. 6). This was especially true at station
561 TYR where the lowest NCP rates were measured. At this station, dust addition whether under
562 present or future conditions of temperature and pH did not switch the community towards net
563 autotrophy but even drove the community towards a stronger heterotrophy. This was related to
564 the fact that while gross primary production rates were not positively impacted, community
565 respiration increased in tanks D and G. At station ION, dust addition alone (tanks D) led to a
566 switch from net heterotrophy to net autotrophy after two days of incubation due to a stronger
567 positive effect of dust on GPP than on CR. Under future environmental conditions (tanks G), the
568 same observation was made with higher NCP and GPP rates than in tanks D. CR rates reacted
569 quickly to these forcing factors in tanks G and initially (first incubation) drove the community
570 towards a much stronger heterotrophy as compared to the other tanks. Finally, at station FAST,
571 similarly to what was observed at ION, the community became autotrophic after two days of
572 incubation in dust amended tanks as, although both GPP and CR were positively impacted by
573 dust addition, this impact was less important for CR. Warming and acidification had a limiting
574 impact on this enhancement, with a lower final NCP in tanks G compared to tanks D, a
575 difference that can be related to an absence of effects of these environmental stressors on GPP
576 while CR clearly increased at higher temperature and lower pH.
577 While BP remained constant or gradually increased in control tanks depending on the
578 station, a clear and quick fertilization effect was observable following dust addition (treatment D

579 and G) at all stations (Fig. 7). At station TYR, BP rates sharply increased to reach maximal
580 values at t24h, with an even stronger increase observed under warmer and acidified conditions
581 (tanks G). After this initial increase, rates slightly decreased towards the end of the experiment.
582 This fertilization effect appeared less important at station ION where lower maximal rates were
583 obtained after 24 h as compared to station TYR. Nevertheless, the same observations can be
584 made, namely, 1) higher rates were measured under future temperature and pH levels and 2) after
585 this initial sharp increase, rates gradually decreased towards the end of the experiment especially
586 in tanks G. At station FAST, a much stronger effect of warming/acidification was observed with
587 an important increase of BP in tanks G until 24 or 48 h post-seeding, depending on the duplicate.
588 A sharp decline was observed for this treatment until the end of the experiment although rates
589 remained higher than those measured in tanks C and D. The impact of dust addition under
590 present environmental conditions (tanks D) was somehow more limited than at the other stations
591 with a gradual increase until t72h with maximal rates ~ 40 - 100% higher than rates measured in
592 the controls. However, BP increased exponentially between t0 and t12h in all tanks including
593 controls, and in all experiments (Table 2). The growth rate of BP (μ_{BP}) in control tanks was the
594 highest at TYR, intermediate at ION and the lowest at FAST. μ_{BP} increased significantly in all
595 dust amended tanks compared to controls. Under future environmental scenarios, μ_{BP} tended to
596 increase compared to treatment D but with a variable relative change (Table 2).
597 BGE increased in dust amended tanks under present environmental conditions (treatment
598 D) at TYR and ION, while no changes were detectable at station FAST due to a strong
599 discrepancy between control duplicates and overall higher BGE at this station in the controls
600 (Table 3). In contrast, warming and acidification exerted the strongest effect at station FAST
601 with a doubling of BGE between treatment G and D. Although an increase in BGE was also

observed at the two other stations in treatment G as compared to present environmental conditions (treatment D), this increase was more limited (ca. 1 to 1.4-fold increase).

The alkaline phosphatase Vm (AP Vm) increased in all experiments after dust seeding, with amplified effects in G treatments (Fig. S4). Note that AP Vm increased also in the controls at TYR and FAST. In contrast, leucine aminopeptidase Vm (LAP vm) showed succession of peaks instead of a continuously increase (Fig. S4). It was higher in dust alone treatment (D) as compared to the controls at TYR and FAST. A larger variability between duplicates at ION prevents such an observation. At all stations, maximum velocities were measured under future environmental conditions (G). Vm being possibly influenced by enzyme synthesis but also by the number of cells inducing such enzymes, we computed also specific AP Vm per heterotrophic bacterial cell (Fig. 7). Specific AP Vm slightly increased during all experiments in controls and dust-amended tanks (D) with no visible differences between these treatments, a clear over-expression of this enzyme was observed under warmer and more acidified conditions (treatment G) especially at station FAST where velocities were enhanced by a ~8-fold at t96h.

3.4. Inorganic and organic material export

Both total mass and organic matter fluxes, as measured from analyses of the sediment traps at the end of each experiment, were extremely low under control conditions (Fig. 8). Only less than 30% of the dust introduced at the surface of the tanks were recovered at the end of the experiment (3 or 4 days after) in the sediment traps with TYR>ION>FAST. The composition of the exported material was quite similar for each experiment with no significant difference between D and G treatments with 3-5% opal, 4% organic matter, 35-36% $CaCO_3$ and 48-54% lithogenic (Fig. S5). Additions of dust in tanks D and G led to a strong increase in both fluxes with a large variability between the duplicates of treatment D at ION. No clear changes between

625 tanks maintained under present and future conditions of temperature and pH could be
626 highlighted.

4. Discussion

4.1. Initial conditions of the tested waters and evolution in controls

As discussed in details in the companion paper from Gazeau et al. (2021), the three sampling stations were typical of stratified (mixed layer depth of 10-20 m) oligotrophic conditions encountered in the open Mediterranean Sea in late spring / early summer. Briefly, the low NO_x:DIP ratios nutrient concentrations suggest that communities found at the three stations experienced N and P co-limitation at the start of the experiments. The composition of the smaller size phytoplankton communities differed substantially, with autotrophic nano-eukaryotes dominating at stations TYR and ION and a larger contribution from autotrophic pico-eukaryotes and Cyanobacteria at station FAST. The observed low total chlorophyll *a* concentrations and the small contribution of large phytoplankton cells at the start of the three experiments are characteristic of LNLC areas in general, and of surface Mediterranean waters in late spring and summer (Siokou-Frangou et al., 2010). DOC concentrations at the start of the experiments were in the same range (60 - 75 μmol C L^{-1}) as those measured from samples collected in surface waters using clean sampling procedures (Van Wambeke et al., 2021), revealing no contamination issues from our sampling device. TAA concentrations as measured in the tanks at t0 were also consistent with measurements from surface water samples (Van Wambeke et al., 2021) with an average across stations and treatments of 254 ± 36 nmol L^{-1} (Fig. S2). In contrast, TCHO appeared higher at t0 (average across stations and treatments of 681 ± 98 nmol L^{-1}) than concentrations based on clean *in situ* sampling (average of 595 ± 43 nmol L^{-1}; Van Wambeke et al., 2021). The decrease in POC concentrations between pumping (t-12h) and t0 for the three

649 experiments, especially at station TYR (likely linked to higher initial concentrations), was likely
650 a consequence of sedimentation of senescent cells and/or fecal pellets in our experimental
651 systems, which are designed to evaluate the export of matter thanks to their conical shape. TEP
652 concentrations were not quantified at t-12h and therefore there is no possibility to evaluate if
653 sedimentation of these particles occurred before t0 in our tanks. At t0, larger and more abundant
654 TEP were measured at station TYR compared to the two other stations (data not shown).
655 As a consequence of a very low availability in inorganic nutrients, TChl*a* and ^{14}C-based
656 production rates were very low, all typical of oligotrophic conditions. Nano- and micro-
657 phytoplanktonic cells (> 2 µm) contributed most of the ^{14}C-based particulate production (~ 80%),
658 as found also on several on-deck incubations at the three stations (on average 73 ± 6%; Marañón
659 et al., 2021). %PER values were also very similar to those measured during these on-deck
660 incubations (~ 40-45%; see Marañón et al., 2021). This suggests no significant impact of our
661 experimental protocol on rates and partitioning of ^{14}C-based production rates (i.e. sampling from
662 the continuous seawater supply, delay of 12 h before initial measurements, artificial light etc.).
663 The low values of chlorophyll stocks as well as of ^{14}C-based production rates are consistent with
664 previous estimates based on direct measurements, satellite observations and modelling
665 approaches in the same areas in late spring / early summer (e.g. Bosc et al., 2004; Lazzari et al.,
666 2016; Moutin and Raimbault, 2002).
667 The metabolic balance was in favor of net heterotrophy at all stations at the start of the
668 experiments (NCP < 0). Net heterotrophy in the open Mediterranean sea at this period of the year
669 has been reported by Regaudie-de-Gioux et al. (2009) and Christaki et al. (2011) in agreement
670 with our measurements at t0 in control tanks (Table 1). The lowest NCP and the highest CR rates
671 were measured at station TYR, suggesting that the autotrophic plankton community was not very

672 active at this station. This was confirmed by the ^{14}C-based particulate production rates, which
673 were about half the ones measured at the other two stations. The community at TYR was most
674 likely relying on regenerated nutrients, as shown by the highest levels of ammonium (NH_4^+)
675 measured at the start of this experiment (Gazeau et al., 2021). As discussed in Guieu et al.
676 (2020a), a dust deposition event took place several days before the arrival of the vessel in this
677 area, likely on May 10-12. This dust event was confirmed by inventory of particulate aluminium
678 in the water column at several stations of the Tyrrhenian Sea including TYR, 6 to 9 d after the
679 event (Bressac et al., 2021). This dust deposition likely stimulated phytoplankton growth and
680 POC accumulation shortly after the deposition and consequently increased the abundance of
681 herbivorous grazers (copepods) and attracted carnivorous species (Feliú et al., 2020),
682 subsequently driving the community towards a net heterotrophic state that characterized the
683 initial condition of the experiment at this station. The favorable conditions for BP growth at TYR
684 were also confirmed by the highest μ_{BP} growth rates obtained among the three experiments
685 (Table 2; 0.06 - 0.07 h^{-1}) in controls tanks.
686 The two other stations, although both also showing a slight net heterotrophic state, were
687 clearly different from each other in terms of initial biological stocks and metabolic rates. Indeed,
688 whereas TChl*a* and abundances of pico- and nano-autotrophic cells (flow cytometry counts;
689 Gazeau et al., 2021) were higher at FAST compared to ION, the autotrophic community was not
690 more efficient at fixing carbon at FAST, as shown by similar initial ^{14}C-based production rates.
691 In contrast, both heterotrophic prokaryotic abundances and BP were much higher at station
692 FAST as compared to ION, leading to initial higher CR and lower NCP. At ION, the initial NCP
693 closer to metabolic balance further suggests a tight coupling between heterotrophic prokaryotes
694 and phytoplankton at this station, as discussed by Dinasquet et al. (2021).

For most of the chemical and biological stocks (e.g. nutrients, pigments etc.) presented in Gazeau et al. (2021), no major changes took place during the three experiments under control conditions. Here, we further show that DOC, POC as well as TEP concentrations did not exhibit strong changes during the experiments. For DOC, large variability between the duplicates (C1 and C2) potentially masked an increase towards the end of the experiments. The same holds true for autotrophic metabolic rates, as ^{14}C-based particulate production rates showed no marked variations during the three experiments, although a slight increase was visible at FAST until t48h. The communities at the three stations remained heterotrophic under the nutrient-limited conditions in the controls. However, heterotrophic prokaryotes probably benefited from initial inputs of available organic matter issued from other stressed eukaryotic organisms and/or POC decay between t-12h and t0, which could be due to both sedimentation and degradation. This was reflected in the progressive increase of BP, their variable initial growth rates (μ_{BP} ranged from 0.02 to 0.06 h^{-1} in control tanks according to the experiment) as well as increasing TAA/DOC ratios at the three stations. Finally, an initial increase of BP during incubations is generally described and classically attributed to a bottle effect, which favours large, fast-growing bacteria and often induces mortality of some phytoplankton cells (Calvo-Díaz et al., 2011; Ferguson et al., 1984; Zobell and Anderson, 1936)

4.2. Impact of dust addition under present environmental conditions

The addition of nitrogen and phosphorus in the experimental tanks through dust seeding (+ 11 to + 11.6 µmol L^{-1} and + 22 to + 30.8 nmol L^{-1} for NO_x and DIP, respectively, in dust enriched, i.e. D1 and D2, versus controls; Gazeau et al., 2021) had very contrasting impacts on

717 the metabolism of the communities, depending on the station. At TYR, surprisingly, the relieving
718 of nutrient (N, P) limitation had a negative impact on ^{13}C incorporation as well as on both
719 particulate and dissolved ^{14}C-based production rates (as seen by the relative changes compared to
720 the control presented in Fig. 9). These observations are fully corroborated by the observed
721 relative decrease in GPP in these tanks (D1 and D2) relative to controls and by the negative
722 impact of dust-addition on TChl*a* concentrations as discussed by Gazeau et al. (2021). Integrated
723 ^{14}C-incorporation rates converted to P (using a C:P molar ratio of 245:1 determined in the
724 particulate organic matter in surface waters of the Northwestern Mediterranean Sea during
725 stratification; Tanaka et al., 2011) showed that phytoplankton P requirements in treatment D (~2
726 nmol P L^{-1}) were much lower than the release of DIP through dust addition at station TYR (+
727 20.4 to + 24.6 nmol P L^{-1}; Gazeau et al., 2020). This suggests that the observed strong decrease
728 of DIP at TYR following dust addition was due to an utilization by the heterotrophic
729 compartment. Indeed, in contrast to the autotrophic compartment, both heterotrophic prokaryotic
730 abundances (Gazeau et al., 2021) and BP (this study, Fig. 9) showed that heterotrophic
731 prokaryotes reacted quickly and strongly to the increase in DIP availability. Integrated BP
732 increased by almost 400% in tanks D1 and D2 as compared to controls (Fig. 9). Such relative
733 increases of BP surpassing by far the observed relative increases of CR suggest a much more
734 efficient utilization of resources by heterotrophic prokaryotes in this treatment (i.e. BGE
735 increased by 200% as compared to the controls; Fig. 9). As such, at TYR, the addition of dust
736 drove the community to an even more heterotrophic state. Such absence of response of the
737 autotrophic community despite the input of new N and P from simulated wet deposition was
738 never observed in dust enrichment experiments performed in the Mediterranean Sea (Guieu and
739 Ridame, 2020). To the best of our knowledge, it is the first time that a negative effect of dust

addition is experimentally demonstrated on the metabolic balance. The apparent utilization of nutrients, especially DIP (Gazeau et al., 2021), by heterotrophic prokaryotes was extremely fast, starting right after dust addition and driving DIP concentrations back to control levels at the end of the experiment (t72h). While heterotrophic prokaryotic abundances increased until the end of the experiment, BP rates increased exponentially during the first 24h, and then BP reached a plateau. Heterotrophic prokaryotes appeared limited by nutritive resources although DIP concentrations were not yet back to their initial level and no relative increase of the AP Vm per cell compared to the control was observed in these tanks. Independent nutrient experiments showed a direct stimulation of BP in the dark after addition of DIP (Van Wambeke et al., 2021), suggesting a great competition with phytoplankton for DIP utilization at TYR. After 24 h, abundances of heterotrophic prokaryotes continued to increase while BP stabilized, suggesting a less extent of lysis and viral control than in the other experiments (abundances of heterotrophic nanoflagellates decreased; Dinasquet et al., 2021). This limitation of BP was potentially a consequence of relatively less available access to labile DOC sources, as ^{14}C-based production rates decreased relative to the controls at t24h and t48h although BP increased by 200 - 800%. The very tight coupling between phytoplankton and bacteria at all stations investigated was further confirmed by the absence of an important ^{13}C incorporation into DOC (Fig. S3).

At stations ION and FAST, in contrast to TYR, both the autotrophic and heterotrophic community benefited from dust addition relative to the controls (Fig. 9). Interestingly, while the relative increase in integrated autotrophic processes (GPP and all ^{14}C-based production rates) was more important at FAST than at ION, the opposite was observed for BP. Estimated BGE values even suggest an absence of response to dust addition at station FAST compared to the controls. The different (relative) responses of BP at the two stations could be partly explained by

763 the dynamics of BP in the control tanks as no clear pattern could be observed at ION while a
764 continuous increase was observed at FAST. As shown by Gazeau et al. (2021), at FAST,
765 abundances of heterotrophic prokaryotes were much higher at the start of the experiment, further
766 increased until t48h and then declined until the end of the experiment.

767 We can rule out a potential limitation of BP from DIP availability at station FAST as DIP
768 levels remained much higher in tanks D than in the controls (Gazeau et al., 2021). Furthermore,
769 the amount of maximum DIP reached before its decline compared to TYR and ION showed a
770 less important direct DIP uptake, suggesting that communities were not as much P limited at
771 FAST compared to the other stations at the start of the experiment. Finally, no increase of
772 specific AP Vm was observed in these tanks as compared to the controls (Fig. 7), suggesting no
773 particular additional needs for AP synthesis per unit cell following dust addition. A potential
774 explanation resides in the competition between heterotrophic bacteria and phytoplankton for DIP
775 utilization. At station ION, P requirements of the autotrophic community were low compared to
776 the initial input of DIP following dust seeding (~9 nmol P L^{-1} as compared to an input of + 22 to
777 + 23.3 nmol P L^{-1}; Gazeau et al., 2021). In contrast, at FAST, the autotrophic community
778 consumed a much larger proportion of the initial DIP input (~25 nmol P L^{-1} as compared to an
779 input of 30.8 - 31.3 nmol P L^{-1}) and phytoplankton appeared as a winner for the utilization of
780 DIP towards the end of the experiment at this station. It seems that heterotrophic bacteria and
781 phytoplankton were more in balance and less stressed at the start of the experiment at FAST, i.e.
782 phytoplankton abundances showed no decrease between t-12h and t0 and BP did not increase as
783 much as during the other two experiments, suggesting a strong predation pressure (μ_{BP} was the
784 lowest of the three experiments: ca. 0.02 h^{-1} in the controls).

785 The explanation for the observed differential responses of the autotrophic community at
786 the two stations (FAST > ION) is not evident and further complicated by the fact that the
787 sampling strategy differed between the two stations (i.e. no sampling at t72h, replaced by a
788 sampling at t96h). It is however unlikely that this different sampling strategy was responsible for
789 the different changes in computed integrated autotrophic rates at the two stations. As a maximal
790 increase in nano-eukaryote abundance was observed at t72h at FAST (followed by a drastic
791 reduction at t96h; Gazeau et al., 2021), excluding this sampling point in the calculation of
792 autotrophic metabolic rates would most likely have led to an underestimation of these rates rather
793 than an overestimation. Furthermore, a similar partitioning of ^{14}C-based production rates
794 throughout the two experiments did not provide clear insights on which size-group benefited the
795 most at station FAST compared to ION. Two non-exclusive explanations could be proposed: (1)
796 as mentioned above, a less important immediate consumption of DIP by heterotrophic bacteria
797 leading to a higher availability of new DIP for phytoplankton growth at FAST (+ 31 vs + 22 to +
798 23 nmol L^{-1} at FAST and ION, respectively; Gazeau et al., 2021) along with (2) the presence of a
799 potentially more active community at the start of the experiment at FAST with a much higher
800 contribution from smaller cells (i.e. pico-eukaryotes, *Synechococcus*; Gazeau et al., 2021) that
801 are well known to be better competitors for new nutrients (e.g. Moutin et al., 2002) and that were
802 less stressed at the start of the experiments.

803 During both experiments at ION and FAST, communities switched from net heterotrophy
804 to net autotrophy between 48 and 72 h following dust addition (Fig. 6), leading to a positive
805 integrated NCP at both stations (Fig. 9). This is an important observation since, to the best of our
806 knowledge, the present study constitutes the first investigation of the community metabolism
807 response to dust addition. However, it is important to discuss the timing of such a switch in

808 community metabolism. Since heterotrophic prokaryotes reacted faster than autotrophs to the
809 relief of nutrient (N, P) limitation (i.e. BP already increased by 150-500% at t24 h, while ^{14}C-
810 based production rates increased only after 48-72 h), NCP was first lower (and negative) in the
811 dust-amended tanks as compared to the controls. Marañón et al. (2010) and Pulido-Villena
812 (2008, 2014) have already reported on a much faster response of the heterotrophic prokaryote
813 community to dust enrichment in the central Atlantic Ocean and Mediterranean Sea,
814 respectively. As DIP concentrations at the completion of their 48 h incubations did not differ
815 from that in the controls, it is unlikely that primary production rates and consequently NCP
816 would have further increased. In contrast, during our experiments, DIP concentrations in dust-
817 amended tanks (D) reached initial levels only after 72 h at TYR and ION and remained far above
818 ambient levels at FAST until the end of the experiment (t96h). During the PEACETIME cruise,
819 high frequency sampling of CTD casts allowed following the evolution of biogeochemical
820 properties and fluxes before and after wet dust deposition that took place in the area around
821 FAST on June 3-5 (Van Wambeke et al., 2020). As in our experiment, a rapid increase in BP was
822 responsible for the observed *in situ* decline in DIP concentrations in the mixed layer following
823 the rain with no detectable changes in primary production (Van Wambeke et al., 2020). The
824 intensity of the wet deposition event that was simulated during our experiments was, by far,
825 higher, but still representative of a realistic scenario (Bonnet and Guieu, 2006; Loÿe-Pilot and
826 Martin, 1996; Ternon et al., 2010).

827 The most intriguing result concerning the export of inorganic and organic matter is that
828 these fluxes were maximal at the end of the experiment at TYR in the dust-amended tanks
829 despite the fact that ^{14}C-based production was relatively low and not enhanced by dust addition.
830 Based on previous studies (Bressac et al., 2014; Louis et al., 2017; Ternon et al., 2010), organic

matter export was most likely mainly due to the formation of organic-mineral aggregates triggered by the introduced lithogenic particles (referred thereafter to as POC_{litho}). Indeed, Louis et al. (2017) showed that such an aggregation process occurs within 1 h after dust deposition. These authors further demonstrated the key role of TEP as the conversion of dissolved organic matter (DOM) to POC was mediated by TEP formation/aggregation activated by the introduction of dust. As TEP concentrations were only measured on two occasions after seeding with the first measurement occuring at t24h,), it prevents studying in detail the dynamics of these particles. Nevertheless, it is very likely that the sharp decrease of TEP-C (Fig. 3) between t24h and t72h was related to POC_{litho} export. The coefficient linking POC_{litho} to $Litho_{flux}$ (i.e. the mass of sedimented particles) measured here (0.02) is consistent with values reported for other experiments conducted in the Mediterranean Sea (Louis et al., 2017).

Even though ^{14}C-based production rates were enhanced in the dust-amended tanks at stations ION and FAST, the amount of POC exported at the end of these experiments remained lower than at TYR, with fluxes ~ 10-20 mg C m^{-2} d^{-1}.

The recovery of the introduced dust (traced by the lithogenic mass recovered in the traps) was low (27% at TYR, ~20% at ION and 13-19% at FAST) reflecting that a majority of the dust particles (the smaller ones that are the most abundant according to the particle size distribution of the dust) still remained in the tanks after 3 or 4 days following dust addition. This has been already observed in pelagic mesocosms (Bressac et al., 2012) as those small particles can aggregate to organic matter and eventually sink. The higher export efficiency observed (TYR>ION>FAST) is likely linked to the higher initial abundance and higher production of TEPs during the experiment (Fig. 3). At TYR, impacted by a strong dust event several days before the experiment started (see above), the likely stimulation of the autotrophs after this *in*

situ event should have been followed by the production of a fresh and abundant DOM, comparable to the "post-bloom situation" in Bressac and Guieu (2013).

4.3. Impact of dust addition under future environmental conditions

Warming and/or acidification had a clear impact on most evaluated stocks and metabolic rates. Gazeau et al. (2021) have already discussed temperature/pH mediated changes in nutrient uptake rates and autotrophic community composition in these experiments. Briefly, they showed that warming and acidification did not have any detectable impact on the release of nutrients from atmospheric particles. Furthermore, these external drivers did not drastically modify the composition of the autotrophic assemblage with all groups benefiting from warmer and acidified conditions. Here, we showed that the difference in the response of plankton community metabolism to dust addition under present and future conditions of temperature and pH was highly dependent on the sampling station (Fig. 9). At all stations, ^{14}C-based particulate production rates were enhanced under future conditions as compared to those measured under present environmental conditions (treatment D) although this pattern was not observed for ^{13}C incorporation into POC at stations ION and FAST. At ION, no differences could be detected and at FAST an even lower ^{13}C-enrichment was measured at the end of the experiment. These contrasting patterns between ^{14}C-uptake rates and ^{13}C-enrichment of POC are likely explained by the fact that the latter covered the whole experimental period (including dark periods) and represents net community carbon production while ^{14}C-based rates were measured over 8 h incubations in the light, providing an estimate in between gross and net carbon production.

875 Similarly, the heterotrophic compartment was more stimulated, as BP rates increased
876 strongly at all stations under future conditions compared to treatment D. The relatively smaller
877 increase in CR rates, compared to BP, leading to higher BGE suggests a better utilization of
878 resources by heterotrophic prokaryotes under future environmental conditions. Overall, CR was
879 more impacted than GPP, with the consequence that all integrated NCP rates decreased under
880 future environmental conditions compared to present conditions (treatment D). At station TYR,
881 as discussed previously, dust addition under present conditions did not lead to a switch from net
882 heterotrophy to net autotrophy. This pattern was even more obvious under warmer/acidified
883 conditions, with a larger decrease in integrated NCP at this station. The decrease of integrated
884 NCP at station FAST relative to controls, as well as the smaller increase of all ^{14}C-based
885 production rates relative to those observed at station ION must be taken with caution. As already
886 discussed, the fact that for these processes (O_2 metabolism and ^{14}C-incorporation), no samples
887 were taken at FAST at t72h when maximal cell abundances were recorded for all autotrophic
888 groups (pico- and nano-eukaryotes, autotrophic bacteria) must have artificially led to an
889 underestimation of these integrated metabolic rates. The question of the timing appeared even
890 more preponderant under warmer/acidified conditions, especially at station FAST, where the
891 very important increase in BP led to a full consumption of DIP before t48h (Gazeau et al., 2021)
892 and drove the community towards a strong heterotrophy. The metabolic balance further switched
893 to a slight autotrophy at t72h when heterotrophic bacterial activity appeared limited by nutrient
894 availability.

895 Both elevated partial pressure of CO_2 (pCO_2) and warming are major global change
896 stressors impacting marine communities. Elevated pCO_2 may directly facilitate oceanic primary
897 production through enhanced photosynthesis (Hein and Sand-Jensen, 1997; Riebesell et al.,

2007) although the effects appear to be species- and even strain-specific (e.g. Langer et al., 2009). Warming affects organisms by enhancing their metabolic rates (Brown et al., 2004; Gillooly et al., 2001). Although recent studies suggest large differences in temperature sensitivity between phytoplankton taxa (Chen and Laws, 2017) and no significant overall difference between algae and protozoa (Wang et al., 2019), mineralization rates are usually believed to be more impacted by warming than primary production rates, potentially leading to a decline in net oceanic carbon fixation (Boscolo-Galazzo et al., 2018; Garcia-Corral et al., 2017; Lopez-Urrutia and Moran, 2007; Regaudie-de-Gioux and Duarte, 2012) and carbon export efficiency (Cael et al., 2017; Cael and Follows, 2016). Overall, our experimental set-up did not allow discriminating warming from acidification effects, precluding an evaluation of their potential individual impacts. Nevertheless, we could speculate to which extent a 3 ºC warming and a doubling of CO_2 can explain some of the observed differences between D and G (for instance, a 2-fold increase in ^{14}C-based production rates at ION). For photosynthesis, meta-analysis studies indicate minor effects of pCO_2 on most investigated species (Kroeker et al., 2013; Mackey et al., 2015). Recent studies show a strong, although species-dependent, temperature sensitivity of phytoplankton growth (Chen and Laws, 2017; Wang et al., 2019), suggesting that a 3 ºC warming could explain most of the increased carbon fixation in G compared to D. With respect to NCP, our results are in line with the general view and suggest a weakening of the so-called fertilization effect of atmospheric deposition in the coming decades.

In contrast, we did not observe an additional impact of future environmental conditions on the export of organic matter after dust addition as, at each station, this export was of the same order of magnitude for treatments D and G. This result is in agreement with the findings of a similar experiment in coastal Mediterranean waters that considered only pH change (Louis et al.,

2017) but stands in contrast with the findings of Müren et al. (2005) who showed a clear decrease in sedimentation following a 5 °C warming in the Baltic Sea. Only a few studies have addressed the combined effect of both temperature and pH changes on aggregation processes and export but none considered dust as the particulate phase. These studies, focused mainly on the formation of TEP, were inconclusive on the impact of these combined factors (Passow and Carlson, 2012, and references therein). The potential effect of warming and acidification on biogenic carbon export was certainly, over the rather restricted duration of the experiments, insignificant as compared to the large amount of carbon exported through the lithogenic pump. Although a longer experimental period would likely be necessary to clearly support an impact of future conditions on export, those changes occur on a long time scale that cannot be easily mimicked by experimental approaches. Only *in situ* co-located observations (atmospheric flux and export in sediment traps) over long temporal scales would be necessary to ascertain the interactive effects of these stressors at the decadal time scale.

5. Conclusion

Although the three experiments were conducted under rather similar conditions in terms of nutrient availability and chlorophyll stock of the tested seawater, contrasting responses were observed following the simulation of a wet dust deposition event. Under present conditions of temperature and pH, at the site where the community was the most heterotrophic (TYR), no positive impact of new nutrients could be observed on autotrophs, while a fast and strong response of heterotrophic bacteria drove the metabolic balance towards an even more heterotrophic state. The situation was different at the two other stations where a more active autotrophic community responded quickly to the relief in nutrient (N, P) limitation, driving the

943 community to an autotrophic state at the end of these experiments. In all tested waters, an overall
944 faster response of the heterotrophic prokaryote community, as compared to the autotrophic
945 community, was observed after new nutrients were released from dust. Phytoplankton could
946 benefit from nutrient inputs, only if the amount released from dust was enough to sustain both
947 the fast bacterial demand and the delayed one of phytoplankton. As our experimental protocol
948 consisted in simulating a strong, although realistic, wet dust deposition, further work should
949 explore at which flux a wet dust deposition triggers an enhancement of net community
950 production and therefore increases the capacity of the surface oligotrophic ocean to sequester
951 atmospheric CO_2. This question, of the utmost importance in particular for modelling purposes,
952 should be answered through future similar experiments as the ones considered in our study but
953 following a gradient approach of dust fluxes. As a consequence of a stronger sensitivity of
954 heterotrophic prokaryotes to temperature and/or pH, the ongoing warming and acidification of
955 the surface ocean will result in a decrease of the dust fertilization of phytoplankton in the coming
956 decades and a weakening of the atmospheric CO_2 sequestration capacity of the surface
957 oligotrophic ocean. The contrasting results obtained at the three stations during our study will
958 need to be translated into process parameterization. The important dataset presented in this
959 manuscript, covering a variety of tested waters, environmental stressors and responses, will
960 allow such parameterization to be used in biogeochemical models coupled to ocean dynamics in
961 order to depict the spatial and temporal dynamics of stocks and fluxes following dust deposition
962 in surface oligotrophic waters.

Data availability

Underlying research data are being used by researcher participants of the PEACETIME campaign to prepare other manuscripts, and therefore data are not publicly acces- sible at the time of publication. Data will be accessible (http: //www.obs-vlfr.fr/proof/php/PEACETIME/peacetime.phpTS4, https://doi.org/10.17882/75747, Guieu et al., 2020b) once the special issue is completed (all papers should be published by fall 2021).

Author contributions

FG and CG designed and supervised the study. All authors participated in sample analyses. FG wrote the paper with contributions from all authors.

Financial support

This study is a contribution to the PEACETIME project (http://peacetime-project.org), a joint initiative of the MERMEX and ChArMEx components supported by CNRS-INSU, IFREMER, CEA, and Météo-France as part of the programme MISTRALS coordinated by INSU. PEACETIME was endorsed as a process study by GEOTRACES and is a contribution to IMBER and SOLAS International programs. PEACETIME cruise (https://doi.org/10.17600/17000300). The project leading to this publication has received funding from European FEDER Fund under project 1166-39417. The research of EM and MPL was supported by the Spanish Ministry of Science, Innovation and Universities through project POLARIS (Grant No. PGC2018-094553B-I00) and by European Union's H2020 research and innovation programme through project

TRIATLAS (Grant No. 817578). JD was funded by a Marie Curie Actions-International Outgoing Fellowship (PIOF-GA-2013-629378).

Acknowledgments

The authors thank the captain and the crew of the RV "*Pourquoi Pas ?*" for their professionalism and their work at sea. Céline Ridame and Kahina Djaoudi are thanked for their help during sampling, Sophie Guasco and Marc Garel for their help in ectoenzymatic measurements onboard.

References

Behrenfeld, M. J., O'Malley, R. T., Siegel, D. A., McClain, C. R., Sarmiento, J. L., Feldman, G. C., Milligan, A. J., Falkowski, P. G., Letelier, R. M. and Boss, E. S.: Climate-driven trends in contemporary ocean productivity, Nature, 444(7120), 752–755, 2006.

Benner, R. and Strom, M.: A critical evaluation of the analytical blank associated with DOC measurements by high-temperature catalytic oxidation, Mar. Chem., 41(1), 153–160, https://doi.org/10.1016/0304-4203(93)90113-3, 1993.

Bishop, J. K. B., Davis, R. E. and Sherman, J. T.: Robotic observations of dust storm enhancement of carbon biomass in the North Pacific, Science, 298(5594), 817–821, https://doi.org/10.1126/science.1074961, 2002.

Bonnet, S. and Guieu, C.: Atmospheric forcing on the annual iron cycle in the western Mediterranean Sea: A 1-year survey, J. Geophys. Res-Biogeo., 111, C09010, https://doi.org/10.1029/2005JC003213, 2006.

Bonnet, S., Guieu, C., Chiaverini, J., Ras, J. and Stock, A.: Effect of atmospheric nutrients on the autotrophic communities in a low nutrient, low chlorophyll system, Limnol. Oceanogr, 50(6), 1810–1819, https://doi.org/10.4319/lo.2005.50.6.1810, 2005.

Bosc, E., Bricaud, A. and Antoine, D.: Seasonal and interannual variability in algal biomass and primary production in the Mediterranean Sea, as derived from 4 years of SeaWiFS observations, Global Biogeochem. Cy., 18(1), GB1005, https://doi.org/10.1029/2003GB002034, 2004.

Boscolo-Galazzo, F., Crichton, K. A., Barker, S. and Pearson, P. N.: Temperature dependency of metabolic rates in the upper ocean: A positive feedback to global climate change?, Global and Planetary Change, 170, 201–212, https://doi.org/10.1016/j.gloplacha.2018.08.017,

2018.

Bressac, M., Guieu, C., Doxaran, D., Bourrin, F., Obolensky, G., and Grisoni, J.-M.: A mesocosm experiment coupled with optical measurements to assess the fate and sinking of atmospheric particles in clear oligotrophic waters, Geo-Mar. Lett., 32, 153–164, doi:10.1007/s00367-011- 0269-4, 2012.

Bressac, M. and Guieu, C.: Post-depositional processes: What really happens to new atmospheric iron in the ocean's surface?, Global Biogeochem. Cy., 27(3), 859–870, https://doi.org/10.1002/gbc.20076, 2013.

Bressac, M., Guieu, C., Doxaran, D., Bourrin, F., Desboeufs, K., Leblond, N. and Ridame, C.: Quantification of the lithogenic carbon pump following a simulated dust-deposition event in large mesocosms, Biogeosciences, 11(4), 1007–1020, https://doi.org/10.5194/bg-11-1007-2014, 2014.

Bressac, M., Wagener, T., Leblond, N., Tovar-Sánchez, A., Ridame, C., Albani, S., Guasco, S., Dufour, A., Jacquet, S., Dulac, F., Desboeufs, K., and Guieu, C.: Subsurface iron accumulation and rapid aluminium removal in the Mediterranean following African dust deposition, Biogeosciences Discussions, 1–29, https://doi.org/10.5194/bg-2021-87, 2021.

Brown, J. H., Gillooly, J. F., Allen, A. P., Savage, V. M. and West, G. B.: Toward a Metabolic Theory of Ecology, Ecology, 85(7), 1771–1789, https://doi.org/10.1890/03-9000, 2004.

Cael, B. B. and Follows, M. J.: On the temperature dependence of oceanic export efficiency, Geophys. Res. Lett., 43(10), 5170–5175, https://doi.org/10.1002/2016GL068877, 2016.

Cael, B. B., Bisson, K. and Follows, M. J.: How have recent temperature changes affected the efficiency of ocean biological carbon export?, Limnol. Oceanogr. Lett., 2(4), 113–118, https://doi.org/10.1002/lol2.10042, 2017.

Calvo-Díaz, A., Díaz-Pérez, L., Suárez, L. Á., Morán, X. A. G., Teira, E. and Marañón, E.: Decrease in the Autotrophic-to-Heterotrophic Biomass Ratio of Picoplankton in Oligotrophic Marine Waters Due to Bottle Enclosure, Appl. Environ. Microbiol., 77(16), 5739–5746, https://doi.org/10.1128/AEM.00066-11, 2011.

Chen, B. and Laws, E. A.: Is there a difference of temperature sensitivity between marine phytoplankton and heterotrophs?, Limnol. Oceanogr., 62(2), 806–817, https://doi.org/10.1002/lno.10462, 2017.

Christaki, U., Van Wambeke, F., Lefevre, D., Lagaria, A., Prieur, L., Pujo-Pay, M., Grattepanche, J.-D., Colombet, J., Psarra, S., Dolan, J. R., Sime-Ngando, T., Conan, P., Weinbauer, M. G. and Moutin, T.: Microbial food webs and metabolic state across oligotrophic waters of the Mediterranean Sea during summer, Biogeosciences, 8(7), 1839–1852, https://doi.org/10.5194/bg-8-1839-2011, 2011.

Desboeufs, K., Leblond, N., Wagener, T., Bon Nguyen, E. and Guieu, C.: Chemical fate and settling of mineral dust in surface seawater after atmospheric deposition observed from dust seeding experiments in large mesocosms, Biogeosciences, 11(19), 5581–5594, https://doi.org/10.5194/bg-11-5581-2014, 2014.

Desboeufs, K.: Nutrients atmospheric deposition and variability, in Atmospheric Chemistry in the Mediterranean – Vol. 2, From Pollutant Sources to Impacts, edited by Dulac, F., Sauvage, S., and Hamonou, E., Springer, Cham, Switzerland, in press, 2021.

Dinasquet, J., Bigeard, E., Gazeau, F., Azam, F., Guieu, C., Marañón, E., Ridame, C., Van Wambeke, F., Obernosterer, I., and Baudoux, A.-C.: Impact of dust addition on the microbial food web under present and future conditions of pH and temperature, Biogeosciences Discussions, 1–48, https://doi.org/10.5194/bg-2021-143, 2021.

1058 Dittmar, T., Cherrier, J. and Ludwichowski, K.-U.: The analysis of amino acids in seawater, in
1059 Practical Guidelines for the Analysis of Seawater, edited by O. Wurl, pp. 67–77, CRC
1060 Press Taylor & Francis Group, Boca Raton, FL., 2009.
1061 Emerson, S., Quay, P., Karl, D., Winn, C., Tupas, L. and Landry, M.: Experimental
1062 determination of the organic carbon flux from open-ocean surface waters, Nature,
1063 389(6654), 951–954, https://doi.org/10.1038/40111, 1997.
1064 Engel, A.: Determination of marine gel particles, in Practical Guidelines for the Analysis of
1065 Seawater, edited by O. Wurl, pp. 125–142, CRC Press Taylor & Francis Group, Boca
1066 Raton, FL., 2009.
1067 Engel, A. and Händel, N.: A novel protocol for determining the concentration and composition
1068 of sugars in particulate and in high molecular weight dissolved organic matter (HMW-
1069 DOM) in seawater, Mar. Chem., 127(1), 180–191,
1070 https://doi.org/10.1016/j.marchem.2011.09.004, 2011.
1071 Feliú, G., Pagano, M., Hidalgo, P. and Carlotti, F.: Structure and function of epipelagic
1072 mesozooplankton and their response to dust deposition events during the spring
1073 PEACETIME cruise in the Mediterranean Sea, Biogeosciences, 17, 5417–5441,
1074 https://doi.org/10.5194/bg-17-5417-2020, 2020.
1075 Ferguson, R. L., Buckley, E. N. and Palumbo, A. V.: Response of marine bacterioplankton to
1076 differential filtration and confinement., Appl. Environ. Microbiol., 47(1), 49–55, 1984.
1077 Friedlingstein, P., O'Sullivan, M., Jones, M. W., Andrew, R. M., Hauck, J., Olsen, A., Peters, G.
1078 P., Peters, W., Pongratz, J., Sitch, S., Le Quéré, C., Canadell, J. G., Ciais, P., Jackson, R.
1079 B., Alin, S., Aragão, L. E. O. C., Arneth, A., Arora, V., Bates, N. R., Becker, M., Benoit-
1080 Cattin, A., Bittig, H. C., Bopp, L., Bultan, S., Chandra, N., Chevallier, F., Chini, L. P.,

Evans, W., Florentie, L., Forster, P. M., Gasser, T., Gehlen, M., Gilfillan, D., Gkritzalis, T., Gregor, L., Gruber, N., Harris, I., Hartung, K., Haverd, V., Houghton, R. A., Ilyina, T., Jain, A. K., Joetzjer, E., Kadono, K., Kato, E., Kitidis, V., Korsbakken, J. I., Landschützer, P., Lefèvre, N., Lenton, A., Lienert, S., Liu, Z., Lombardozzi, D., Marland, G., Metzl, N., Munro, D. R., Nabel, J. E. M. S., Nakaoka, S.-I., Niwa, Y., O'Brien, K., Ono, T., Palmer, P. I., Pierrot, D., Poulter, B., Resplandy, L., Robertson, E., Rödenbeck, C., Schwinger, J., Séférian, R., Skjelvan, I., Smith, A. J. P., Sutton, A. J., Tanhua, T., Tans, P. P., Tian, H., Tilbrook, B., van der Werf, G., Vuichard, N., Walker, A. P., Wanninkhof, R., Watson, A. J., Willis, D., Wiltshire, A. J., Yuan, W., Yue, X. and Zaehle, S.: Global Carbon Budget 2020, Earth Syst. Sci. Data, 12(4), 3269–3340, https://doi.org/10.5194/essd-12-3269-2020, 2020.

Garcia-Corral, L. S., Holding, J. M., Carrillo-de-Albornoz, P., Steckbauer, A., Pérez-Lorenzo, M., Navarro, N., Serret, P., Gasol, J. M., Morán, X. A. G., Estrada, M., Fraile-Nuez, E., Benítez-Barrios, V., Agusti, S. and Duarte, C. M.: Temperature dependence of plankton community metabolism in the subtropical and tropical oceans, Global Biogeochem. Cy., 31(7), 1141–1154, https://doi.org/10.1002/2017GB005629, 2017.

Gazeau, F., Ridame, C., Van Wambeke, F., Alliouane, S., Stolpe, C., Irisson, J.-O., Marro, S., Grisoni, J.-M., De Liège, G., Nunige, S., Djaoudi, K., Pulido-Villena, E., Dinasquet, J., Obernosterer, I., Catala, P. and Guieu, C.: Impact of dust addition on Mediterranean plankton communities under present and future conditions of pH and temperature: an overview, Biogeosciences, 18, 1–24, https://doi.org/10.5194/bg-18-1-2021, 2021.

Gillikin, D. P. and Bouillon, S.: Determination of $\delta^{18}O$ of water and $\delta^{13}C$ of dissolved inorganic carbon using a simple modification of an elemental analyser-isotope ratio mass

spectrometer: an evaluation, Rapid Commiun. Mass Sp., 21(8), 1475–1478, https://doi.org/10.1002/rcm.2968, 2007.

Gillooly, J. F., Brown, J. H., West, G. B., Savage, V. M. and Charnov, E. L.: Effects of size and temperature on metabolic rate, Science, 293(5538), 2248–2251, https://doi.org/10.1126/science.1061967, 2001.

del Giorgio, P. and Williams, P.: Respiration in Aquatic Ecosystems, Oxford University Press. https://oxford.universitypressscholarship.com/view/10.1093/acprof:oso/9780198527084.001.0001/acprof-9780198527084, last access: 22 January 2021, 2005.

Guieu, C. and Ridame, C.: Impact of atmospheric deposition on marine chemistry and biogeochemistry, in Atmospheric Chemistry in the Mediterranean Region: Comprehensive Diagnosis and Impacts, edited by F. Dulac, S. Sauvage, and E. Hamonou, Springer, Cham, Switzerland, 2020.

Guieu, C., Loye-Pilot, M. D., Benyahya, L. and Dufour, A.: Spatial variability of atmospheric fluxes of metals (Al, Fe, Cd, Zn and Pb) and phosphorus over the whole Mediterranean from a one-year monitoring experiment: Biogeochemical implications, Mar. Chem., 120(1–4), 164–178, https://doi.org/10.1016/j.marchem.2009.02.004, 2010.

Guieu, C., Ridame, C., Pulido-Villena, E., Bressac, M., Desboeufs, K. and Dulac, F.: Impact of dust deposition on carbon budget: a tentative assessment from a mesocosm approach, Biogeosciences, 11(19), 5621–5635, 2014a.

Guieu, C., Aumont, O., Paytan, A., Bopp, L., Law, C. S., Mahowald, N., Achterberg, E. P., Marañón, E., Salihoglu, B., Crise, A., Wagener, T., Herut, B., Desboeufs, K., Kanakidou, M., Olgun, N., Peters, F., Pulido-Villena, E., Tovar-Sanchez, A. and Völker, C.: The significance of the episodic nature of atmospheric deposition to Low Nutrient Low

Chlorophyll regions, Global Biogeochemical Cycles, 28(11), 1179–1198, https://doi.org/10.1002/2014GB004852, 2014b.

Guieu, C., D'Ortenzio, F., Dulac, F., Taillandier, V., Doglioli, A., Petrenko, A., Barrillon, S., Mallet, M., Nabat, P. and Desboeufs, K.: Process studies at the air-sea interface after atmospheric deposition in the Mediterranean Sea: objectives and strategy of the PEACETIME oceanographic campaign (May–June 2017), Biogeosciences, 2020(17), 5563–5585, https://doi.org/10.5194/bg-17-5563-2020, 2020a.

Guieu, C., Desboeufs, K., Albani, S., Alliouane, S., Aumont, O., Barbieux, M., Barrillon, S., Baudoux, A.-C., Berline, L., Bhairy, N., Bigeard. E., Bloss, M., Bressac, M., Brito, J., Carlotti, F., de Liege, G., Dinasquet, J., Djaoudi, K., Doglioli, A., D'Ortenzio, F., Doussin, J.-F., Duforet, L., Dulac, F., Dutay, J.-C., Engel, A., Feliu-Brito, G., Ferre, H., Formenti, P., Fu, F., Garcia, D., Garel, D., Gazeau, F., Giorio, C., Gregori, G., Grisoni, J.-M., Guasco, S., Guittonneau, J., Haëntjens, N., Heimburger, L.-E., Helias, S., Jacquet, S., Laurent, B., Leblond, N., Lefevre, D., Mallet , M., Marañón, E., Nabat, P., Nicosia, A., Obernosterer, I., Perez, L., M., Petrenko, A., Pulido-Villena, E., Raimbault, P., Ridame, C., Riffault, V., Rougier, G., Rousselet, L., Roy-Barman, M., Saiz- Lopez, A., Schmechtig, C., Sellegri, K., Siour, G., Taillandier, V., Tamburini , C., Thyssen, M., Tovar-Sanchez, A., Triquet, S., Uitz, J., Van Wambeke, F., Wagener, T., and Zaencker, B.: Bio- geochemical dataset collected during the PEACETIME cruise, SEANOE [Dataset], https://doi.org/10.17882/75747, 2020b.

Hein, M. and Sand-Jensen, K.: CO_2 increases oceanic primary production, Nature, 388(6642), 526–527, 1997.

Herut, B., Zohary, T., Krom, M. D., Mantoura, R. F. C., Pitta, P., Psarra, S., Rassoulzadegan, F.,

Tanaka, T. and Frede Thingstad, T.: Response of East Mediterranean surface water to Saharan dust: On-board microcosm experiment and field observations, Deep Sea Research Part II: Topical Studies in Oceanography, 52(22), 3024–3040, https://doi.org/10.1016/j.dsr2.2005.09.003, 2005.

Herut, B., Rahav, E., Tsagaraki, T. M., Giannakourou, A., Tsiola, A., Psarra, S., Lagaria, A., Papageorgiou, N., Mihalopoulos, N., Theodosi, C. N., Violaki, K., Stathopoulou, E., Scoullos, M., Krom, M. D., Stockdale, A., Shi, Z., Berman-Frank, I., Meador, T. B., Tanaka, T. and Paraskevi, P.: The potential impact of Saharan dust and polluted aerosols on microbial populations in the East Mediterranean Sea, an overview of a mesocosm experimental approach, Front. Mar. Sci., 3, 226, https://doi.org/10.3389/fmars.2016.00226, 2016.

Hoppe, H.-G.: Significance of exoenzymatic activities in the ecology of brackish water: measurements by means of methylumbelliferyl-substrates, Mar. Ecol. Prog. Ser., 11(3), 299–308, 1983.

IPCC: Climate Change 2013: The Physical Science Basis. Contri- bution of Working Group I to the Fifth Assessment Report of the Intergovernmental Panel on Climate Change, edited by: Stocker, T. F., Qin, D., Plattner, G.-K., Tignor, M., Allen, S. K., Boschung, J., Nauels, A., Xia, Y., Bex, V., and Midgley, P. M., Cambridge University Press, Cambridge, United Kingdom and New York, NY, USA, 1535 pp., 2013.

Irwin, A. J. and Oliver, M. J.: Are ocean deserts getting larger?, Geophys. Res. Lett., 36, L18609, https://doi.org/10.1029/2009gl039883, 2009.

Jickells, T. and Moore, C. M.: The importance of atmospheric deposition for ocean productivity, Annu. Rev. Ecol. Evol. S. , 46(1), 481–501, https://doi.org/10.1146/annurev-ecolsys-

112414-054118, 2015.

Kirchman, D. L., Kemp, P., Sherr, B., Sherr, E. and Cole, J.: Leucine incorporation as a measure of biomass production by heterotrophic bacteria, in Handbook of methods in aquatic microbial ecology, pp. 509–512, CRC Press, https://doi.org/10.1201/9780203752746-59, 1993.

Knap, A., Michaels, A., Close, A., Ducklow, H. and Dickson, A.: Protocols for the Joint Global Ocean Flux Study (JGOFS) Core Measurements, UNESCO 1994., 1996.

Kouvarakis, G., Mihalopoulos, N., Tselepides, A. and Stavrakakis, S.: On the importance of atmospheric inputs of inorganic nitrogen species on the productivity of the Eastern Mediterranean Sea, Global Biogeochem. Cy. , 15(4), 805–817, https://doi.org/10.1029/2001GB001399, 2001.

Kroeker, K. J., Kordas, R. L., Crim, R., Hendriks, I. E., Ramajo, L., Singh, G. S., Duarte, C. M. and Gattuso, J. P.: Impacts of ocean acidification on marine organisms: quantifying sensitivities and interaction with warming, Glob. Change Biol., 19(6), 1884–1896, https://doi.org/10.1111/gcb.12179, 2013.

Langer, G., Nehrke, G., Probert, I., Ly, J. and Ziveri, P.: Strain-specific responses of *Emiliania huxleyi* to changing seawater carbonate chemistry, Biogeosciences, 6(11), 2637–2646, https://doi.org/10.5194/bg-6-2637-2009, 2009.

Laurent, B., Audoux, T., Bibi, M., Dulac, F. and Bergametti, G.: Mass deposition in the Mediterranean region, in Atmospheric Chemistry in the Mediterranean Region: Comprehensive Diagnosis and Impacts, edited by F. Dulac, S. Sauvage, and E. Hamonou, Springer, Cham, Switzerland, 2021.

Lazzari, P., Solidoro, C., Salon, S. and Bolzon, G.: Spatial variability of phosphate and nitrate in

the Mediterranean Sea: A modeling approach, Deep-Sea Res. Pt I, 108, 39–52, https://doi.org/10.1016/j.dsr.2015.12.006, 2016.

Lekunberri, I., Lefort, T., Romero, E., Vázquez-Domínguez, E., Romera-Castillo, C., Marrasé, C., Peters, F., Weinbauer, M. and Gasol, J. M.: Effects of a dust deposition event on coastal marine microbial abundance and activity, bacterial community structure and ecosystem function, J. Plankton Res., 32(4), 381–396, https://doi.org/10.1093/plankt/fbp137, 2010.

Lemée, R., Rochelle-Newall, E., Van Wambeke, F., Pizay, M., Rinaldi, P. and Gattuso, J.-P.: Seasonal variation of bacterial production, respiration and growth efficiency in the open NW Mediterranean Sea, Aquat. Microb. Ecol., 29, 227–237, https://doi.org/10.3354/ame029227, 2002.

Lewandowska, A. M., Boyce, D. G., Hofmann, M., Matthiessen, B., Sommer, U. and Worm, B.: Effects of sea surface warming on marine plankton, Ecol. Lett., 17(5), 614–623, https://doi.org/10.1111/ele.12265, 2014.

Lindroth, P. and Mopper, K.: High performance liquid chromatographic determination of subpicomole amounts of amino acids by precolumn fluorescence derivatization with o-phthaldialdehyde, Anal. Chem., 51(11), 1667–1674, https://doi.org/10.1021/ac50047a019, 1979.

Longhurst, A., Sathyendranath, S., Platt, T. and Caverhill, C.: An estimate of global primary production in the ocean from satellite radiometer data, J. Plankton Res., 17(6), 1245–1271, https://doi.org/10.1093/plankt/17.6.1245, 1995.

Lopez-Urrutia, A. and Moran, X. A. G.: Resource limitation of bacterial production distorts the temperature dependence of oceanic carbon cycling, Ecology, 88(4), 817–822, 2007.

Louis, J., Pedrotti, M. L., Gazeau, F. and Guieu, C.: Experimental evidence of formation of transparent exopolymer particles (TEP) and POC export provoked by dust addition under current and high pCO_2 conditions, PLOS ONE, 12(2), e0171980, https://doi.org/10.1371/journal.pone.0171980, 2017.

Loÿe-Pilot, M. D. and Martin, J. M.: Saharan Dust Input to the Western Mediterranean: An Eleven Years Record in Corsica, in The Impact of Desert Dust Across the Mediterranean, edited by S. Guerzoni and R. Chester, pp. 191–199, Springer Netherlands, Dordrecht, https://doi.org/10.1007/978-94-017-3354-0_18, 1996.

Mackey, K., Morris, J. J., Morel, F. and Kranz, S.: Response of photosynthesis to ocean acidification, Oceanography, 25(2), 74–91, https://doi.org/10.5670/oceanog.2015.33, 2015.

Marañón, E., Fernández, A., Mouriño-Carballido, B., MartÍnez-GarcÍa, S., Teira, E., Cermeño, P., Chouciño, P., Huete-Ortega, M., Fernández, E., Calvo-DÍaz, A., Morán, X. A. G., Bode, A., Moreno-Ostos, E., Varela, M. M., Patey, M. D. and Achterberg, E. P.: Degree of oligotrophy controls the response of microbial plankton to Saharan dust, Limnol. Oceanogr., 55(6), 2339–2352, https://doi.org/10.4319/lo.2010.55.6.2339, 2010.

Marañón, E., Lorenzo, M. P., Cermeño, P. and Mouriño-Carballido, B.: Nutrient limitation suppresses the temperature dependence of phytoplankton metabolic rates, The ISME Journal, 12(7), 1836–1845, https://doi.org/10.1038/s41396-018-0105-1, 2018.

Marañón, E., Van Wambeke, F., Uitz, J., Boss, E. S., Dimier, C., Dinasquet, J., Engel, A., Haëntjens, N., Pérez-Lorenzo, M., Taillandier, V., and Zäncker, B.: Deep maxima of phytoplankton biomass, primary production and bacterial production in the Mediterranean Sea, Biogeosciences, 18, 1749–1767, https://doi.org/10.5194/bg-18-1749-

2021, 2021.

Mari, X.: Carbon content and C:N ratio of transparent exopolymeric particles (TEP) produced by bubbling exudates of diatoms, Mar. Ecol. Prog. Ser., 183, 59–71, https://doi.org/10.3354/meps183059, 1999.

Markaki, Z., Oikonomou, K., Kocak, M., Kouvarakis, G., Chaniotaki, A., Kubilay, N. and Mihalopoulos, N.: Atmospheric deposition of inorganic phosphorus in the Levantine Basin, eastern Mediterranean: Spatial and temporal variability and its role in seawater productivity, Limnol. Oceanogr., 48(4), 1557–1568, https://doi.org/10.4319/lo.2003.48.4.1557, 2003.

Maugendre, L., Gattuso, J.-P., Louis, J., de Kluijver, A., Marro, S., Soetaert, K. and Gazeau, F.: Effect of ocean warming and acidification on a plankton community in the NW Mediterranean Sea, ICES J. Mar. Sci., 72(6), 1744–1755, https://doi.org/10.1093/icesjms/fsu161, 2015.

Maugendre, L., Gattuso, J.-P., Poulton, A. J., Dellisanti, W., Gaubert, M., Guieu, C. and Gazeau, F.: No detectable effect of ocean acidification on plankton metabolism in the NW oligotrophic Mediterranean Sea: Results from two mesocosm studies, Estuar. Coast. Shelf S., 186, 89–99, https://doi.org/10.1016/j.ecss.2015.03.009, 2017a.

Maugendre, L., Guieu, C., Gattuso, J.-P. and Gazeau, F.: Ocean acidification in the Mediterranean Sea: Pelagic mesocosm experiments. A synthesis, Estuar. Coast. Shelf S., 186, 1–10, https://doi.org/10.1016/j.ecss.2017.01.006, 2017b.

McClain, C. R., Signorini, S. R., and Christian, J. R.: Subtropical gyre variability observed by ocean-color satellites, Deep-Sea Res. Pt II, 51, 281–301, https://doi.org/10.1016/j.dsr2.2003.08.002, 2004.

Mercado, J. M., Sobrino, C., Neale, P. J., Segovia, M., Reul, A., Amorim, A. L., Carrillo, P., Claquin, P., Cabrerizo, M. J., León, P., Lorenzo, M. R., Medina-Sánchez, J. M., Montecino, V., Napoleon, C., Prasil, O., Putzeys, S., Salles, S. and Yebra, L.: Effect of CO_2, nutrients and light on coastal plankton. II. Metabolic rates, Aquat. Biol., 22, 43–57, https://doi.org/10.3354/ab00606, 2014.

Mills, M. M., Moore, C. M., Langlois, R., Milne, A., Achterberg, E., Nachtigall, K., Lochte, K., Geider, R. J. and La, R. J.: Nitrogen and phosphorus co-limitation of bacterial productivity and growth in the oligotrophic subtropical North Atlantic, Limnol. Oceanogr., 53(2), 824–834, https://doi.org/10.4319/lo.2008.53.2.0824, 2008.

Mosseri, J., Quéguiner, B., Rimmelin, P., Leblond, N. and Guieu, C.: Silica fluxes in the northeast Atlantic frontal zone of Mode Water formation (38°–45°N, 16°–22°W) in 2001–2002, J. Geophys. Res-Oceans, 110, C07S19, https://doi.org/10.1029/2004JC002615, 2005.

Moulin, C. and Chiapello, I.: Impact of human-induced desertification on the intensification of Sahel dust emission and export over the last decades, Geophys. Res. Lett., 33(18), L18808, https://doi.org/10.1029/2006GL025923, 2006.

Moutin, T. and Raimbault, P.: Primary production, carbon export and nutrients availability in western and eastern Mediterranean Sea in early summer 1996 (MINOS cruise), J. Mar. Syst., 33–34, 273–288, https://doi.org/10.1016/S0924-7963(02)00062-3, 2002.

Moutin, T., Thingstad, T. F., Wambeke, F. V., Marie, D., Slawyk, G., Raimbault, P. and Claustre, H.: Does competition for nanomolar phosphate supply explain the predominance of the cyanobacterium Synechococcus?, Limnol. Oceanogr., 47(5), 1562–1567, https://doi.org/10.4319/lo.2002.47.5.1562, 2002.

1288 Müren, U., Berglund, J., Samuelsson, K. and Andersson, A.: Potential Effects of Elevated Sea-
1289 Water Temperature on Pelagic Food Webs, Hydrobiologia, 545(1), 153–166,
1290 https://doi.org/10.1007/s10750-005-2742-4, 2005.
1291 Passow, U. and Carlson, C. A.: The biological pump in a high CO_2 world, Mar. Ecol. Prog. Ser.,
1292 470, 249–271, 2012.
1293 Polovina, J. J., Howell, E. A. and Abecassis, M.: Ocean's least productive waters are expanding,
1294 Geophys. Res. Lett., 35(3), L03618, https://doi.org/10.1029/2007gl031745, 2008.
1295 Pulido-Villena, E., Wagener, T. and Guieu, C.: Bacterial response to dust pulses in the western
1296 Mediterranean: Implications for carbon cycling in the oligotrophic ocean, Global
1297 Biogeochem. Cy., 22, GB1020, https://doi.org/10.1029/2007gb003091, 2008
1298 Pulido-Villena, E., Baudoux, A.-C., Obernosterer, I., Landa, M., Caparros, J., Catala, P.,
1299 Georges, C., Harmand, J. and Guieu, C.: Microbial food web dynamics in response to a
1300 Saharan dust event: results from a mesocosm study in the oligotrophic Mediterranean
1301 Sea, Biogeosciences, 11(19), 5607–5619, 2014.
1302 Regaudie-de-Gioux, A. and Duarte, C. M.: Temperature dependence of planktonic metabolism in
1303 the ocean, Global Biogeochem. Cy., 26(1), GB1015,
1304 https://doi.org/10.1029/2010GB003907, 2012.
1305 Regaudie-de-Gioux, A., Vaquer-Sunyer, R. and Duarte, C. M.: Patterns in planktonic
1306 metabolism in the Mediterranean Sea, Biogeosciences, 6(12), 3081–3089,
1307 https://doi.org/10.5194/bg-6-3081-2009, 2009.
1308 Ridame, C. and Guieu, C.: Saharan input of phosphate to the oligotrophic water of the open
1309 western Mediterranean Sea, Limnol. Oceanogr., 47(3), 856–869, 2002.

Riebesell, U., Schulz, K. G., Bellerby, R. G. J., Botros, M., Fritsche, P., Meyerhofer, M., Neill, C., Nondal, G., Oschlies, A., Wohlers, J. and Zollner, E.: Enhanced biological carbon consumption in a high CO_2 ocean, Nature, 450(7169), 545-U10, 2007.

Roshan, S. and DeVries, T.: Efficient dissolved organic carbon production and export in the oligotrophic ocean, Nat. Commun., 8, 2036, https://doi.org/10.1038/s41467-017-02227-3, 2017.

Schimmelmann, A., Qi, H., Coplen, T. B., Brand, W. A., Fong, J., Meier-Augenstein, W., Kemp, H. F., Toman, B., Ackermann, A., Assonov, S., Aerts-Bijma, A. T., Brejcha, R., Chikaraishi, Y., Darwish, T., Elsner, M., Gehre, M., Geilmann, H., Gröning, M., Hélie, J.-F., Herrero-Martín, S., Meijer, H. A. J., Sauer, P. E., Sessions, A. L., and Werner, R. A.: Organic Reference Materials for Hydrogen, Carbon, and Nitrogen Stable Isotope-Ratio Measurements: Caffeines, n-Alkanes, Fatty Acid Methyl Esters, Glycines, L-Valines, Polyethylenes, and Oils, Anal. Chem., 88, 4294–4302, https://doi.org/10.1021/acs.analchem.5b04392, 2016.

Schneider, C. A., Rasband, W. S., and Eliceiri, K. W.: NIH Image to ImageJ: 25 years of Image Analysis, Nat. Methods, 9, 671–675, 2012.

Smith, D. C. and Azam, F.: A simple, economical method for measuring bacterial protein synthesis rates in seawater using ^{3}H-leucine, Marine Microbial Food Webs, 6(2), 107–114, 1992.

Tanaka, T., Thingstad, T. F., Christaki, U., Colombet, J., Cornet-Barthaux, V., Courties, C., Grattepanche, J.-D., Lagaria, A., Nedoma, J., Oriol, L., Psarra, S., Pujo-Pay, M. and Wambeke, F. V.: Lack of P-limitation of phytoplankton and heterotrophic prokaryotes in surface waters of three anticyclonic eddies in the stratified Mediterranean Sea,

Biogeosciences, 8(2), 525–538, https://doi.org/10.5194/bg-8-525-2011, 2011.

Ternon, E., Guieu, C., Loÿe-Pilot, M.-D., Leblond, N., Bosc, E., Gasser, B., Miquel, J.-C. and Martín, J.: The impact of Saharan dust on the particulate export in the water column of the North Western Mediterranean Sea, Biogeosciences, 7(3), 809–826, https://doi.org/10.5194/bg-7-809-2010, 2010.

Thingstad, T. F., Krom, M. D., Mantoura, R. F. C., Flaten, G. a. F., Groom, S., Herut, B., Kress, N., Law, C. S., Pasternak, A., Pitta, P., Psarra, S., Rassoulzadegan, F., Tanaka, T., Tselepides, A., Wassmann, P., Woodward, E. M. S., Riser, C. W., Zodiatis, G. and Zohary, T.: Nature of Phosphorus Limitation in the Ultraoligotrophic Eastern Mediterranean, Science, 309(5737), 1068–1071, https://doi.org/10.1126/science.1112632, 2005.

Van Wambeke, F., Taillandier, V., Deboeufs, K., Pulido-Villena, E., Dinasquet, J., Engel, A., Marañón, E., Ridame, C., and Guieu, C.: Influence of atmospheric deposition on biogeochemical cycles in an oligotrophic ocean system, Biogeosciences Discuss. [preprint], https://doi.org/10.5194/bg-2020-411, in review, 2020.

Van Wambeke, F., Pulido, E., Catala, P., Dinasquet, J., Djaoudi, K., Engel, A., Garel, M., Guasco, S., Marie, B., Nunige, S., Taillandier, V., Zäncker, B., and Tamburini, C.: Spatial patterns of ectoenzymatic kinetics in relation to biogeochemical properties in the Mediterranean Sea and the concentration of the fluorogenic substrate used, Biogeosciences, 18, 2301–2323, https://doi.org/10.5194/bg-18-2301-2021, 2021.

Wang, Q., Lyu, Z., Omar, S., Cornell, S., Yang, Z. and Montagnes, D. J. S.: Predicting temperature impacts on aquatic productivity: Questioning the metabolic theory of ecology's "canonical" activation energies, Limnol. Oceanogr., 64(3), 1172–1185,

https://doi.org/10.1002/lno.11105, 2019.

Zobell, C. E. and Anderson, D. Q.: Observations on the multiplication of bacteria in different volumes of stored sea water and the influence of oxygen tension and solid surfaces, The Biological Bulletin, 71(2), 324–342, https://doi.org/10.2307/1537438, 1936.

Tables

Table 1. Initial chemical and biological stocks as measured while filling the tanks (initial conditions in pumped surface water; sampling time: t-12h). NO_x: nitrate + nitrite, DIP: dissolved inorganic phosphorus, $Si(OH)_4$: silicate, POC: particulate organic carbon, DOC: dissolved organic carbon, TEP: transparent exopolymer particles, TChl*a*: total chlorophyll *a*. Values shown for ^{14}C incorporation rates, percentages of extracellular release (%PER) as well as for net community production (NCP), community respiration (CR) and gross primary production (GPP) were estimated from samples taken at t0 in the control tanks. For heterotrophic bacterial production (BP), rates were estimated from seawater sampled at t-12h.

	Sampling station	TYR	ION	FAST
	Coordinates (decimal)	39.34 N, 12.60 E	35.49 N, 19.78 E	37.95 N, 2.90 N
	Bottom depth (m)	3395	3054	2775
	Day and time of pumping (local time)	17/05/2017 17:00	25/05/2017 17:00	02/06/2017 21:00
	Temperature (°C)	20.6	21.2	21.5
	Salinity	37.96	39.02	37.07
Stocks	NO_x (nmol L^{-1})	14.0	18.0	59.0
	DIP (nmol L^{-1})	17.1	6.5	12.9
	$Si(OH)_4$ (µmol L^{-1})	1.0	0.96	0.64

	POC (µmol L^{-1})	12.9	8.5	6.0
	DOC (µmol L^{-1})	72.2	70.2	69.6
	TEP (x 10^6 L^{-1})	6.8	3.8	3.7
	TChl*a* (µg L^{-1})	0.063	0.066	0.072
	Heterotrophic prokaryotes abundance (x 10^5 cell mL^{-1})	4.79	2.14	6.15
Processes	^{14}C-based total particulate production (µg C L^{-1} h^{-1})	0.08 ± 0.03	0.14 ± 0.04	0.15 ± 0.04
	^{14}C-based > 2 µm particulate production (µg C L^{-1} h^{-1})	0.07 ± 0.02	0.11 ± 0.02	0.11 ± 0.02
	^{14}C-based < 2 µm particulate production (µg C L^{-1} h^{-1})	0.01 ± 0.01	0.04 ± 0.02	0.05 ± 0.01
	%PER	60 ± 20	45 ± 3	32 ± 23
	NCP (µmol O_2 L^{-1} d^{-1})	-1.9 ± 0.3	-0.2 ± 0.2	-0.8 ± 0.9
	CR (µmol O_2 L^{-1} d^{-1})	-2.6 ± 0.1	-1.2 ± 0.5	-1.9 ± 1.6
	GPP (µmol O_2 L^{-1} d^{-1})	0.7 ± 0.4	1.1 ± 0.3	1.1 ± 0.7
	BP (ng C L^{-1} h^{-1})	11.6	15.2	34.6

1367

Table 2. Heterotrophic bacterial production (BP) growth rates (μ_{BP} in h^{-1}) estimated from the exponential phase of BP growth, observable from at least four sampling points, between t0 and t12h, during the three experiments (TYR, ION and FAST) in the six tanks (controls: C1, C2; dust addition under present conditions of temperature and pH: D1, D2; dust addition under future conditions of temperature and pH: G1 and G2). Values ± SE are shown.

	μ_{BP}		
	TYR	ION	FAST
C1	0.076 ± 0.025	0.042 ± 0.007	0.020 ± 0.003
C2	0.066 ± 0.018	0.041 ± 0.005	0.026 ± 0.004
D1	0.117 ± 0.008	0.095 ± 0.020	0.089 ± 0.014
D2	0.194 ± 0.020	0.145 ± 0.007	0.090 ± 0.007
G1	0.164 ± 0.020	0.126 ± 0.011	0.124 ± 0.005
G2	0.150 ± 0.003	0.137 ± 0.033	0.163 ± 0.014

1374 Table 3. Estimated bacterial growth efficiency (BGE in %) during the course of the three
1375 experiments (TYR, ION and FAST) in the six tanks (controls: C1, C2; dust addition under
1376 present conditions of temperature and pH: D1, D2; dust addition under future conditions of
1377 temperature and pH: G1 and G2). BGE was calculated based on integrated heterotrophic
1378 bacterial production (BP) and community respiration (CR) rates by applying a bacterial
1379 respiration to CR ratio of 0.7 and a respiratory quotient of 0.8 (see Material and Methods).

	Bacterial growth efficiency (BGE)		
	TYR	ION	FAST
C1	11.1	9.8	15.4
C2	11.7	14.5	22.0
D1	31.8	21.0	17.3
D2	32.3	30.6	19.9
G1	39.3	35.2	37.6
G2	32.5	34.8	38.1

1380

1381

Figure caption

Fig. 1. Location of the sampling stations in the Mediterranean Sea on board the R/V *Pourquoi Pas?* during the PEACETIME cruise (10 May to 11 June 2017). Background shows satellite-derived surface chlorophyll *a* concentration averaged over the entire duration of the cruise (courtesy of Louise Rousselet).

Fig. 2. Dissolved organic carbon (DOC) concentrations and ratio between total hydrolysable amino acids (TAA) and DOC concentrations measured in the six tanks (controls: C1, C2; dust addition under present conditions of temperature and pH: D1, D2; dust addition under future conditions of temperature and pH: G1 and G2) during the three experiments (TYR, ION and FAST). The dashed vertical line indicates the time of seeding (after t0).

Fig. 3. Particulate organic carbon (POC) concentrations and transparent exopolymer particle carbon content (TEP-C) measured in the six tanks (controls: C1, C2; dust addition under present conditions of temperature and pH: D1, D2; dust addition under future conditions of temperature and pH: G1 and G2) during the three experiments (TYR, ION and FAST). The dashed vertical line indicates the time of seeding (after t0).

Fig. 4. ^{14}C-based production rates (A: < 2 μm and B: > 2 μm size fractions, C: total particulate) estimated from 8 h incubations on samples taken in the six tanks (controls: C1, C2; dust addition under present conditions of temperature and pH: D1, D2; dust addition under future conditions of temperature and pH: G1 and G2) during the three experiments (TYR, ION and FAST). The percentage of extracellular release (D, %PER) is also shown.

1402 Fig. 5. Incorporation of ^{13}C into particulate organic carbon ($\delta^{13}C$-POC) in the six tanks (controls:
1403 C1, C2; dust addition under present conditions of temperature and pH: D1, D2; dust addition
1404 under future conditions of temperature and pH: G1 and G2) during the three experiments (TYR,
1405 ION and FAST). The dashed vertical line indicates the time of seeding (after t0).

1406 Fig. 6. A: Net community production (NCP), B: community respiration (CR) and C: gross
1407 primary production (GPP) rates estimated using the oxygen light-dark method (24 h incubations)
1408 on samples taken in the six tanks (C1, C2, D1, D2, G1 and G2) during the three experiments
1409 (TYR, ION and FAST).

1410 Fig. 7. Heterotrophic bacterial production rates (BP) and cell-specific maximum hydrolysis
1411 velocity (Vm) of the alkaline phosphatase (both over 1-2 h incubations) on samples taken in the
1412 six tanks (C1, C2, D1, D2, G1 and G2) during the three experiments (TYR, ION and FAST).

1413 Fig. 8. Total mass and organic matter fluxes measured in the sediment traps at the end of the
1414 three experiments (TYR, ION and FAST) in the six tanks (C1, C2, D1, D2, G1 and G2).

1415 Fig. 9. Relative difference (%) between integrated rates measured in tanks D (D1, D2; dust
1416 addition under present conditions of temperature and pH) and G (G1, G2; dust addition under
1417 future conditions of temperature and pH) as compared to the controls (C1, C2) during the three
1418 experiments (TYR, ION and FAST). Vertical boxes represent the range observed between the
1419 two replicates per treatment.

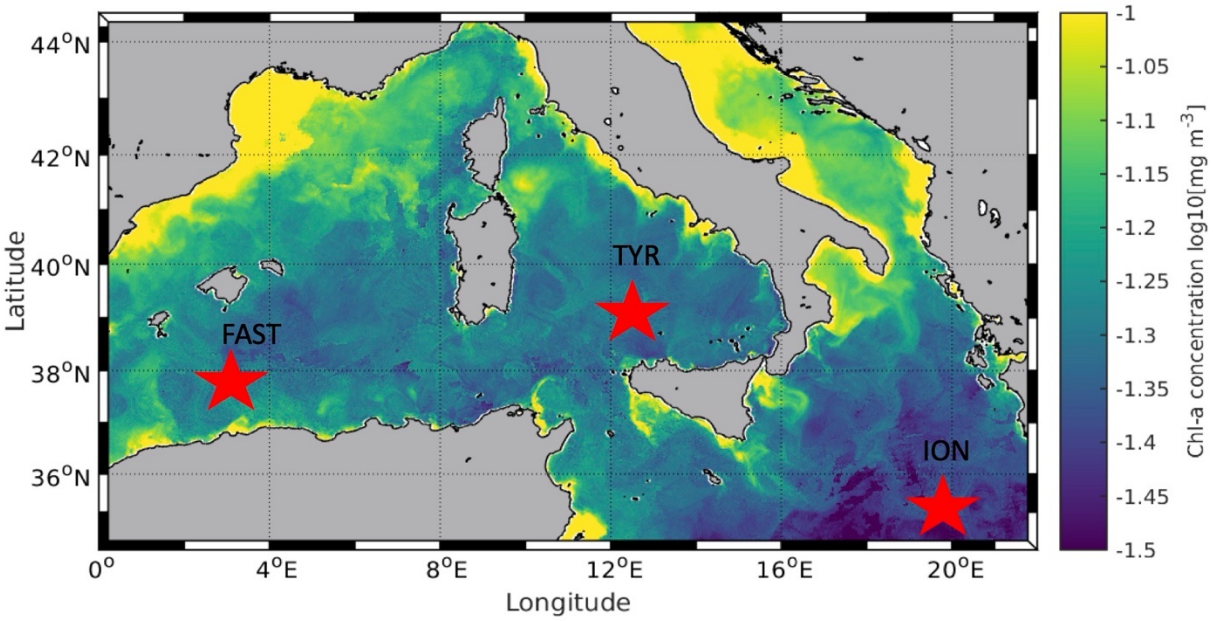

1420

1421 Fig. 1

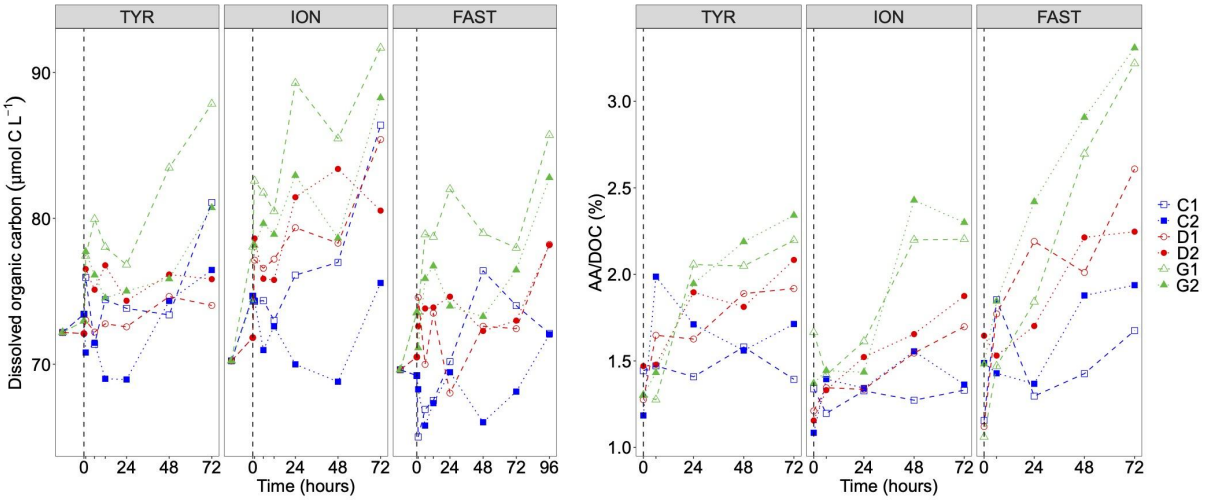

1422

1423 Fig. 2

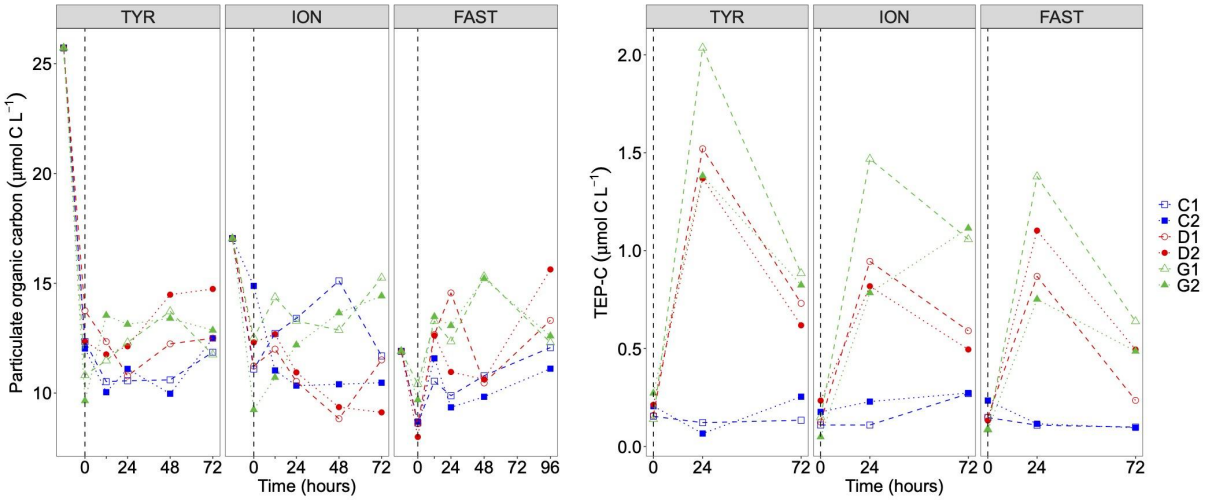

1424

1425 Fig. 3

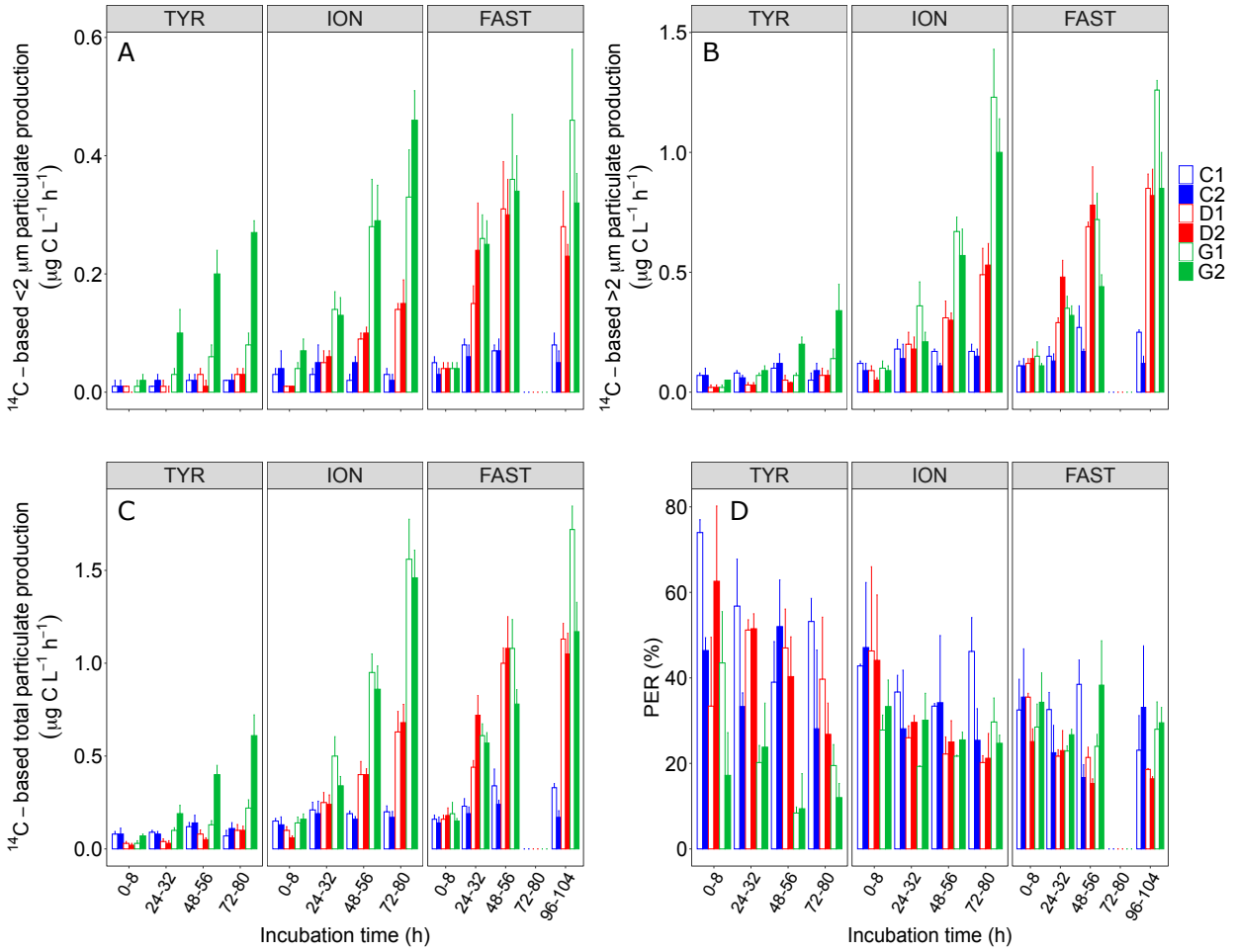

1426

1427 Fig. 4

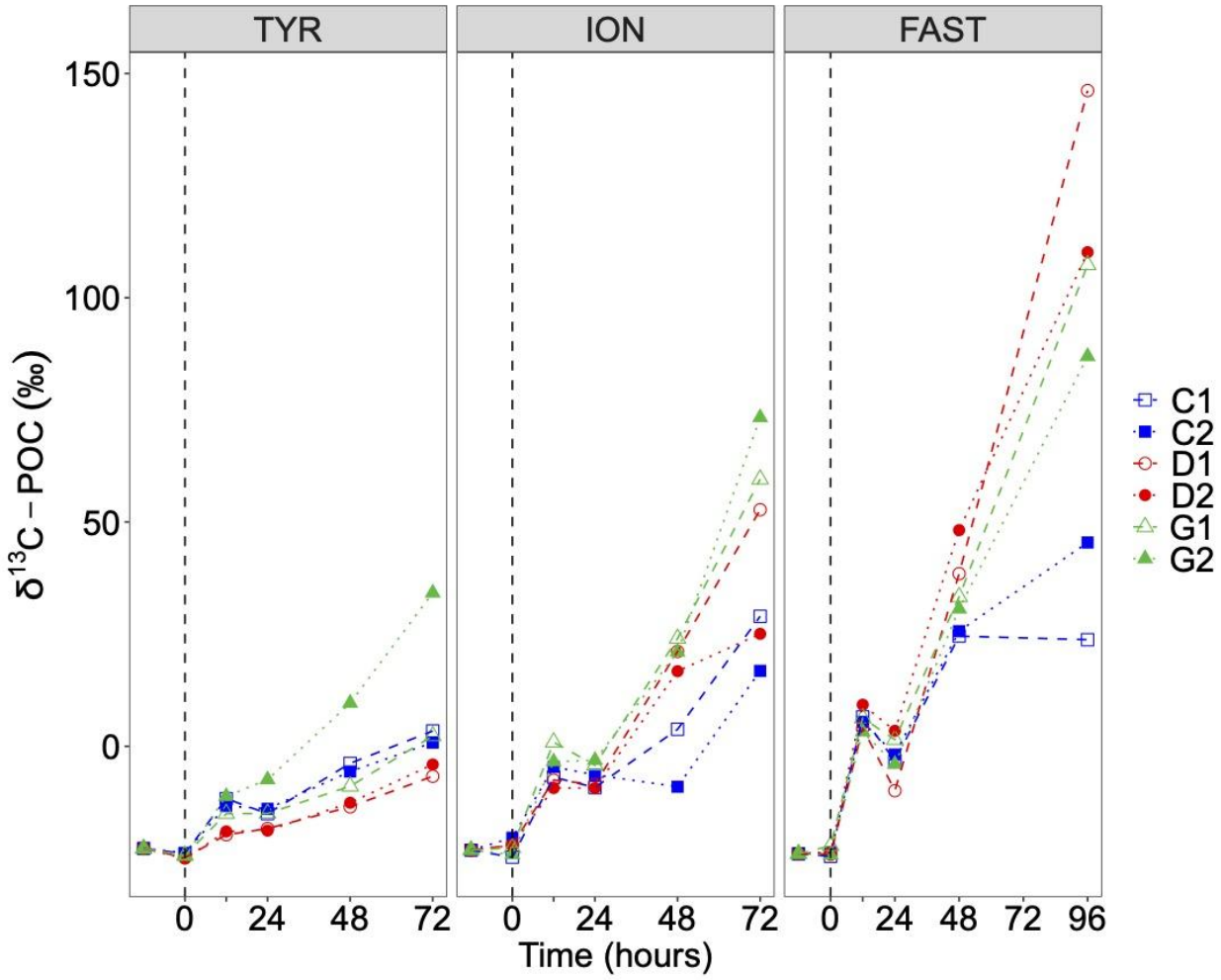

1428

1429 Fig. 5

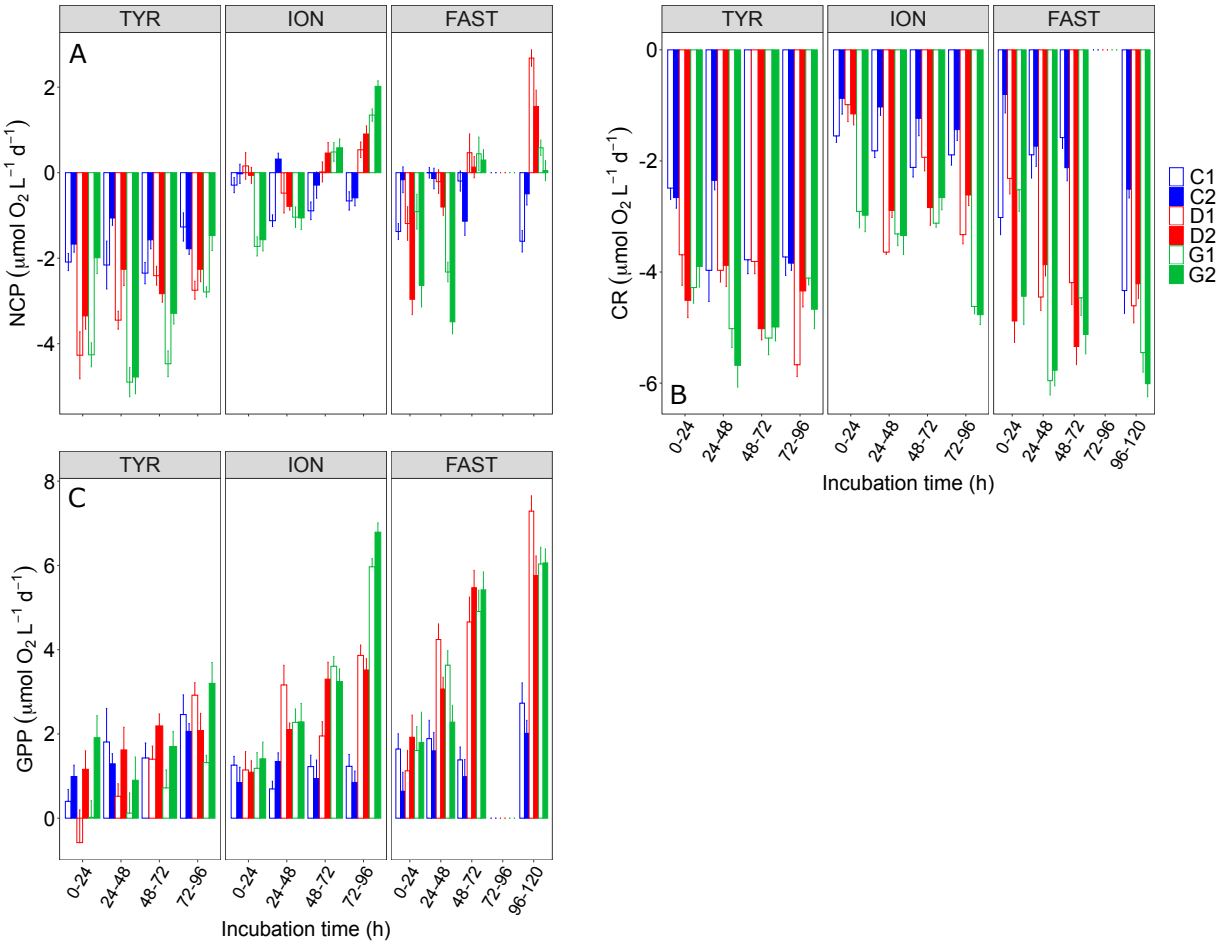

1430

1431 Fig. 6

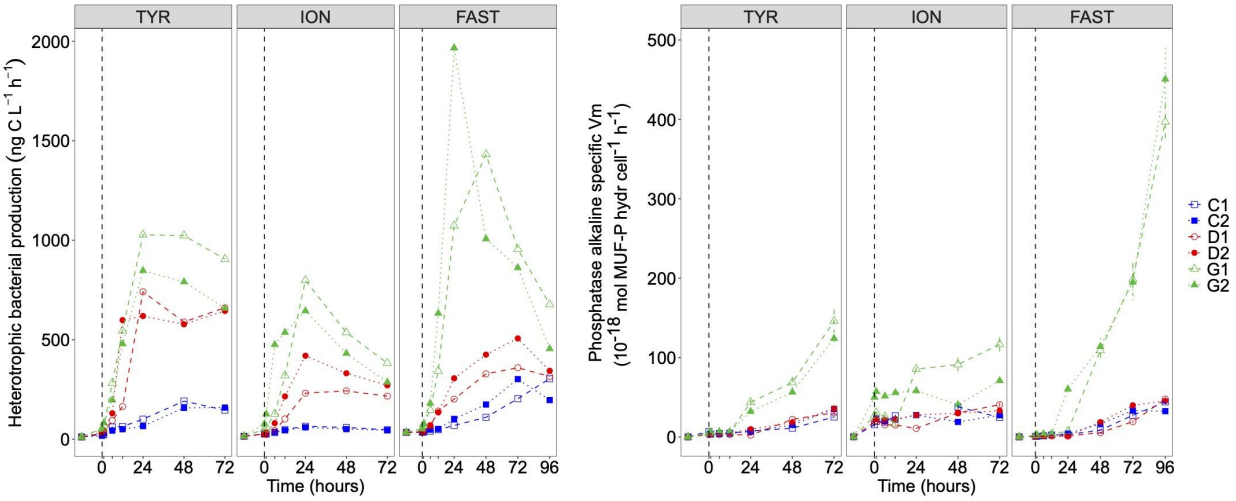

1432

1433 Fig. 7

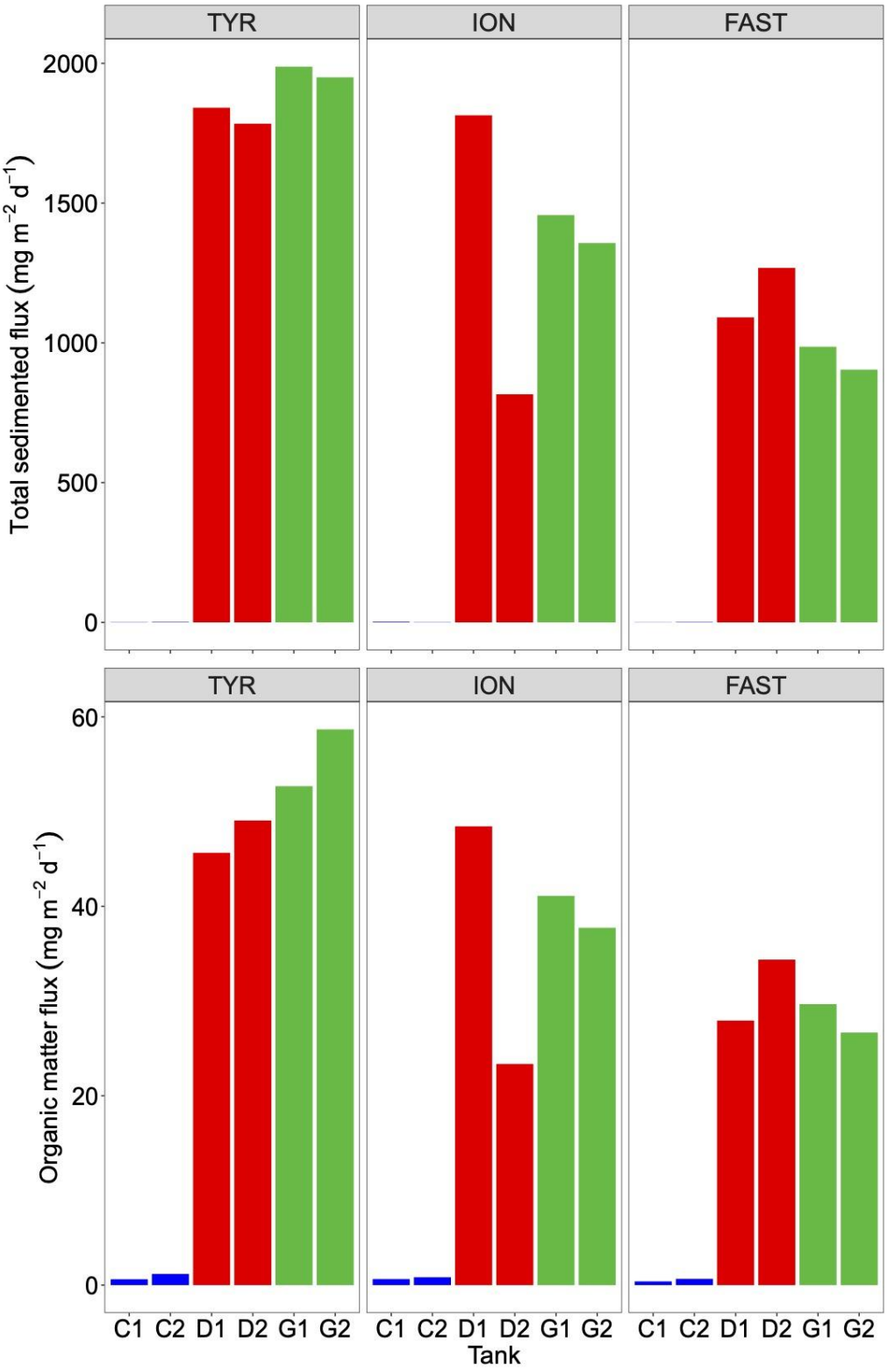

1434

1435 Fig. 8

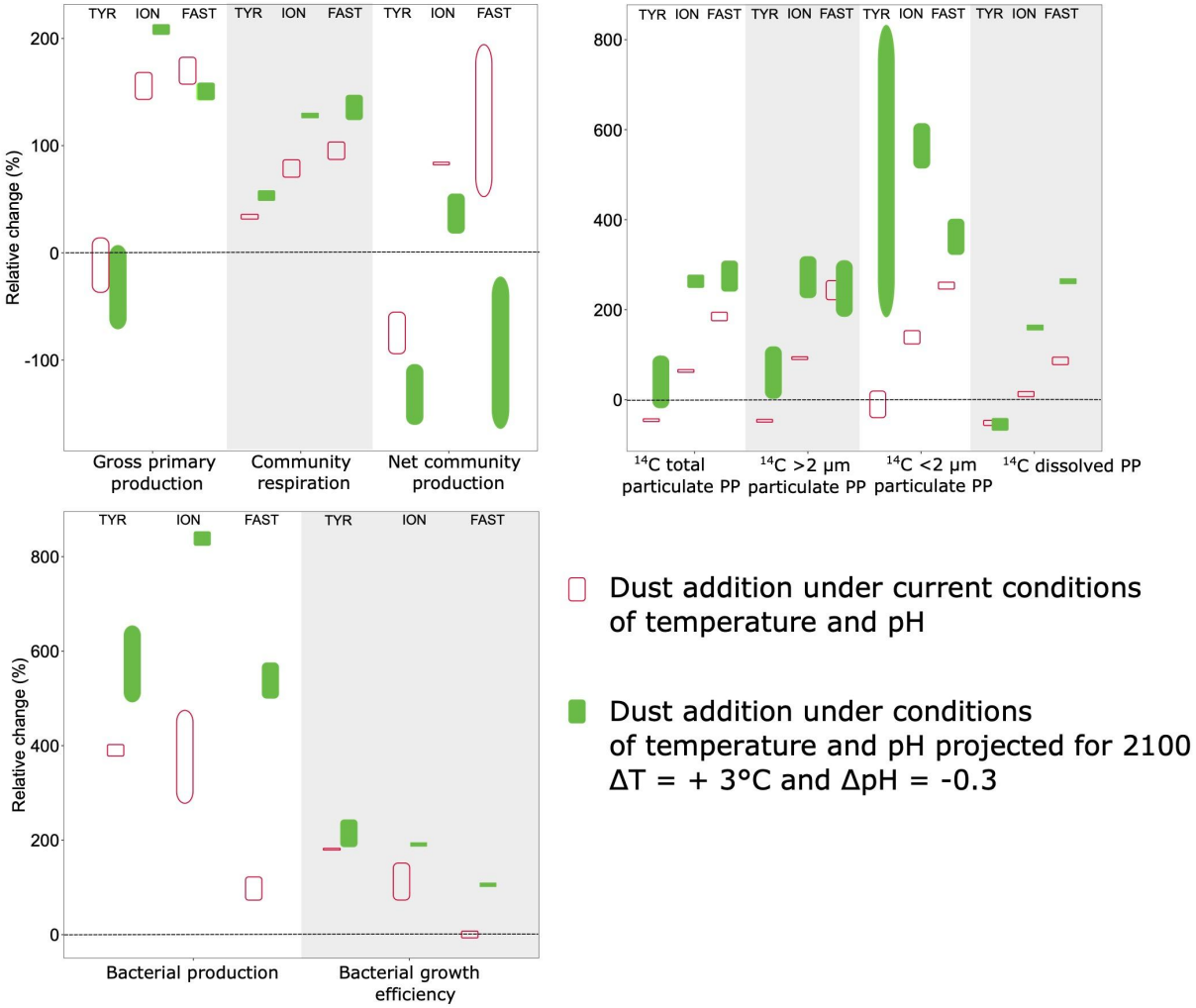

1436

1437 Fig. 9

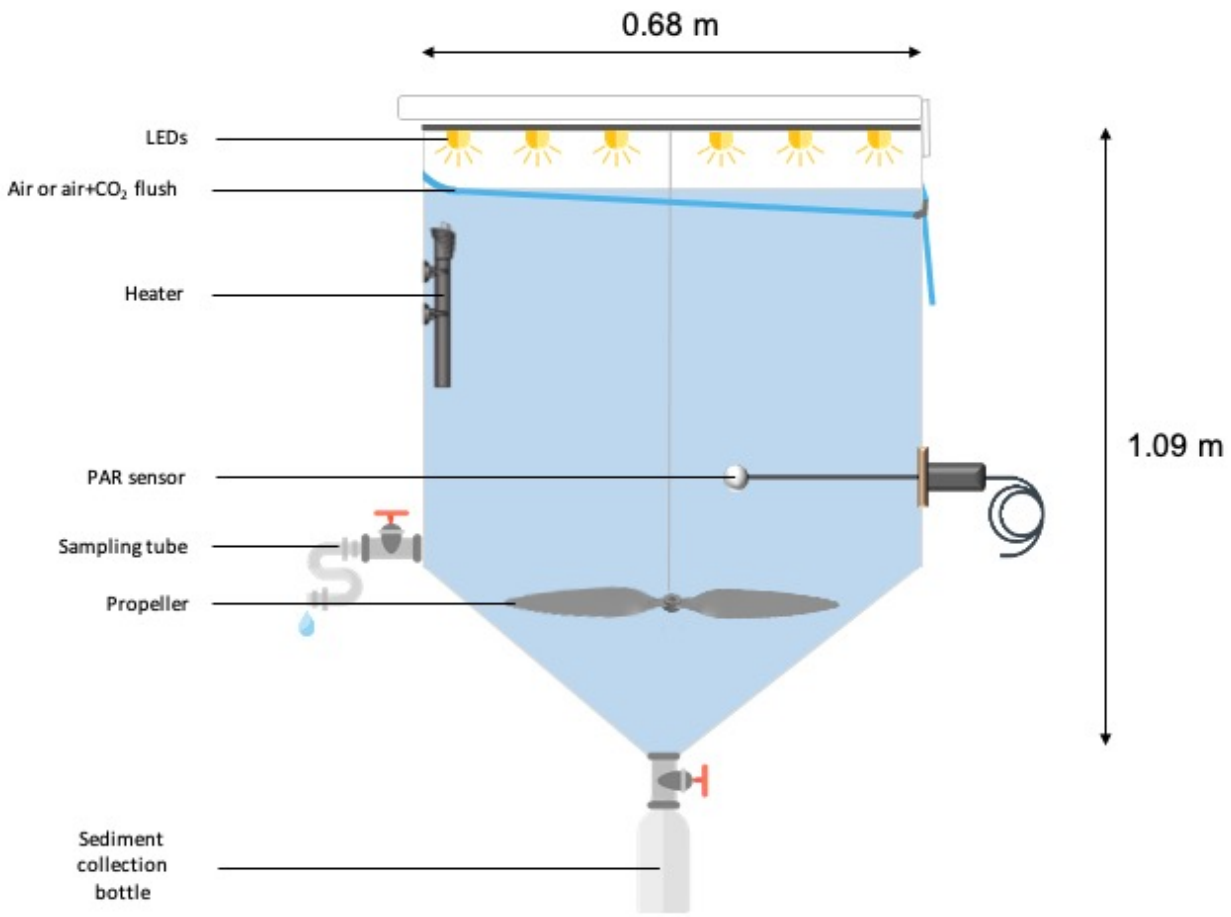

Fig. S1. Diagram of an experimental tank.

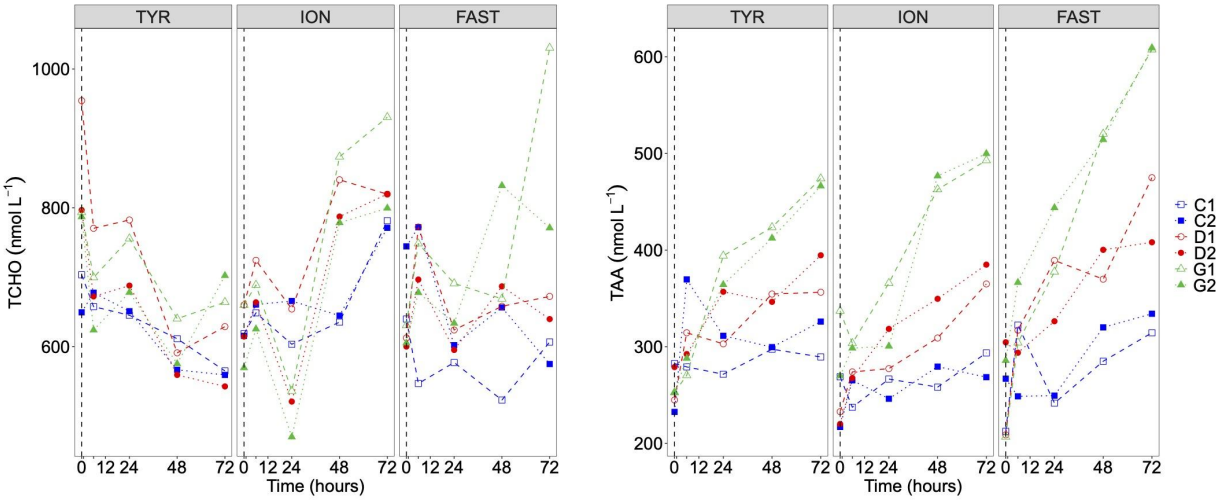

1440

1441 Fig. S2. Total hydrolysable carbohydrate (TCHO) and amino acids (TAA) concentrations in the

1442 six tanks (controls: C1, C2; dust addition under present conditions of temperature and pH: D1,

1443 D2; dust addition under future conditions of temperature and pH: G1 and G2) during the three

1444 experiments (TYR, ION and FAST). The dashed vertical line indicates the time of seeding (after

1445 t0).

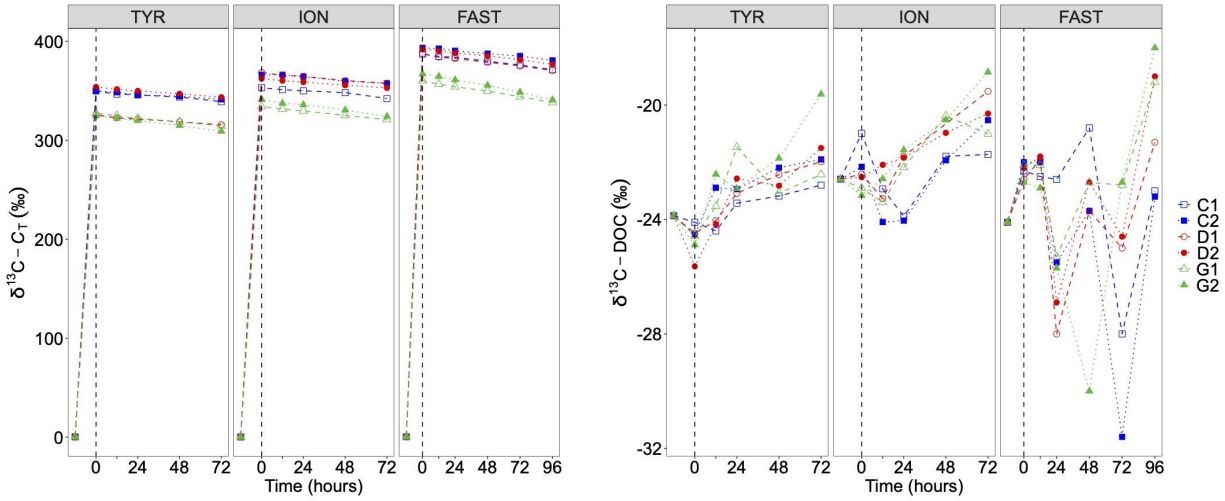

Fig. S3. Isotopic signature of dissolved inorganic carbon (δ^{13}C-C_T) and incorporation of ^{13}C into dissolved organic carbon (δ^{13}C-DOC) in the six tanks (controls: C1, C2; dust addition under present conditions of temperature and pH: D1, D2; dust addition under future conditions of temperature and pH: G1 and G2) during the three experiments (TYR, ION and FAST). The dashed vertical line indicates the time of seeding (after t0).

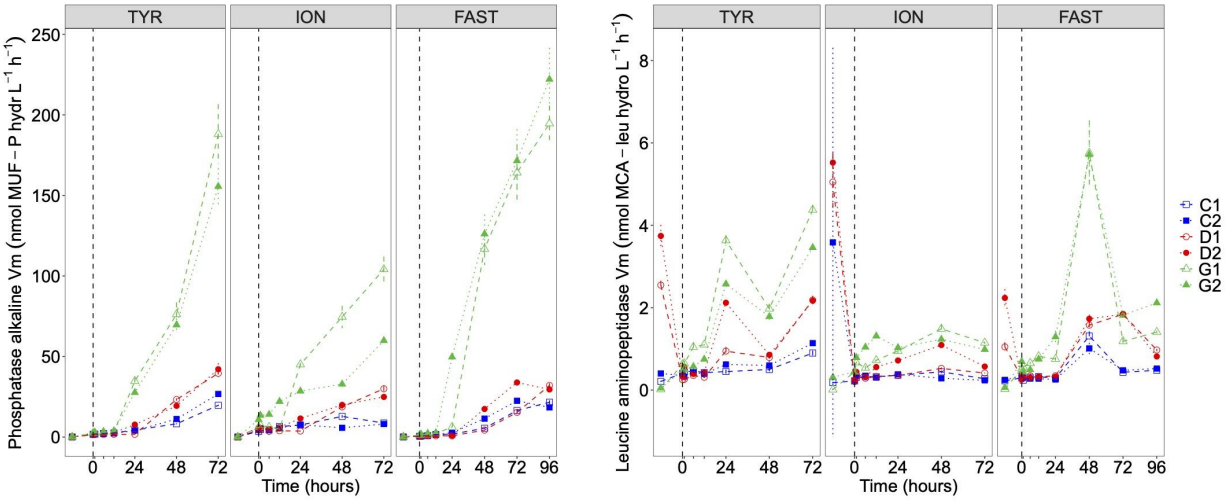

1452

1453 Fig. S4. Maximum hydrolysis velocity (Vm) of the phosphatase alkaline and leucine

1454 aminopeptidase (over 1-2 h incubations) on samples taken in the six tanks (controls: C1, C2; dust

1455 addition under present conditions of temperature and pH: D1, D2; dust addition under future

1456 conditions of temperature and pH: G1 and G2) during the three experiments (TYR, ION and

1457 FAST).

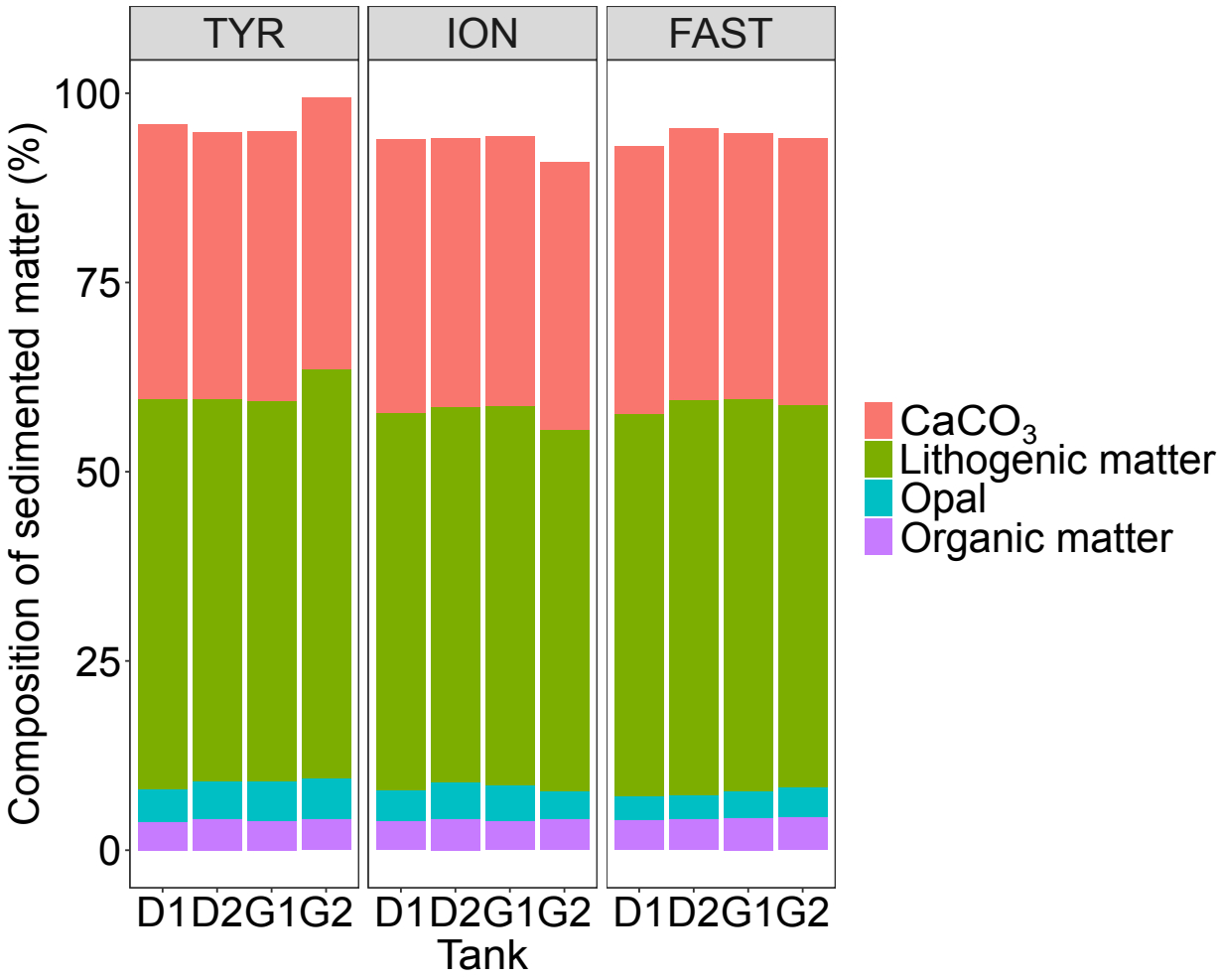

1458

1459 Fig. S5. Proportion (%) of the different fractions analyzed in the recovered sedimented matter at

1460 the end of the three experiments (TYR, ION and FAST) in dust enriched minicosms (D1, D2, G1

1461 and G2).